Sound Radiation Characteristics Of Rectangular Duct

Raviprolu Praveena

ME11M14

A Dissertation Submitted to

Indian Institute of Technology Hyderabad

In Partial Fulfillment of the Requirements for

The Degree of Master of Technology

भारतीय प्रौद्योगिकी संस्थान हैदराबाद
Indian Institute of Technology Hyderabad

Department of Mechanical Engineering

July, 2013

Declaration

I declare that this written submission represents my ideas in my own words, and where others' ideas or words have been included, I have adequately cited and referenced the original sources. I also declare that I have adhered to all principles of academic honesty and integrity and have not misrepresented or fabricated or falsified any idea/data/fact/source in my submission. I understand that any violation of the above will be a cause for disciplinary action by the Institute and can also evoke penal action from the sources that have thus not been properly cited, or from whom proper permission has not been taken when needed.
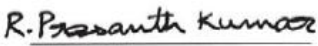
R.Praveena

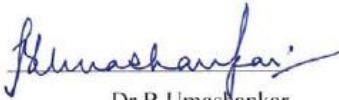(Signature)

Raviprolu Praveena

(ME11M14)

Approval Sheet

This thesis entitled "Sound Radiation Characteristics of Rectangular Duct" by Raviprolu Praveena is approved for the degree of Master of Technology from IIT Hyderabad.

R. Prasanth Kumar

Dr.R. Prasanth Kumar
Assistant Professor IITH
Examiner

B. Venkatesham

Dr.B.Venkatesham
Assistant Professor IITH
Adviser

B. Umashankar

Dr.B.Umashankar
Assistant Professor IITH
Chairman

iii

Acknowledgements

I take this opportunity to thank all the persons who stood behind me in completion of thesis.

First of all I would like to express my sincere and heartfelt thanks to my guide Dr.B.Venkatesham without whose support this thesis could have been incomplete. He has been very supportive throughout my entire work with timely guidance and valuable suggestions.

Heartfelt thanks to my lovely parents, sister and brother-in-law for their support and encouragement.

I would like to thank each and every faculty of my department for their guidance throughout my course work. I would like to thank IIT Hyderabad for providing resources in carrying out my research work.

I would like to thank workshop in charge Mr.Satyanarayana and workshop personnel Mr.Madhu, Mr.Brahmachari, Mr.Ashok, Mr.Jagadeeshan, Mr.Kiran Kumar, Mr. Praveen and every other workshop personnel without whose help the set up for experiment could not have been completed. I extend my thanks to all my lab mates Sachin, Nagaraj, Tapan, Vishal, Ashwin, Girish and Ajay for their support in experimental work. I am very much thankful to my dear friends Shwetha, Naveena, Swasti, Archana, Neetu & Karthika for their support and making my stay in IITH one of the most memorable ones. I am very much thankful to my classmates Jabir, Gyan, Vishwajeet and all my other batch mates. I am also thankful to each and every member of IIT Hyderabad who had been supportive throughout my stay here for the last two years.

Raviprolu Praveena

Dedicated to

My Family and Friends

Abstract

Heating Ventilation and Air Conditioning systems consists of ducts that are made of thin sheets with flexible vibrating walls. These ducts are efficiently designed to supply conditioned air from one location to the other to ensure comfort living of the occupants. During this process, these ducts also carry some amount of noise generated by air-handling units (AHU). Propagating noise in a duct is radiated out along the axial direction and also in transverse direction through the duct walls.

Current research work is focused on understanding the sound radiation characteristics from the rectangular duct walls by understanding the uncoupled and coupled behavior of the structural and acoustic subsystems. A complete analytical, numerical and experimental study has been conducted on a rectangular duct to understand various physical phenomena and to estimate various acoustical and structural parameters.

Theoretical validation studies have been conducted for the proposed equivalent model of a rectangular duct. Numerical sound radiation model of the rectangular duct results are in good agreement with theoretical model results. Radiation modes of the duct have been studied to understand the behavior of the duct in terms of equivalent sound sources such as monopole & dipole. An experimental set up and measurement methodology has been developed for a selected geometry of the duct for measuring structural and acoustic parameters. Experimental results are corroborated with theoretical and numerical results.

Nomenclature

x, y, z   Coordinates of duct dimensions in Numerical model

x_1, x_2, x_3 Coordinates of duct dimensions in Analytical model

E, υ, ρ_s Young's modulus,poisons ratio and density of structural material

c_0, ρ_0 Speed and density of sound in air

a, b   Dimensions of the plate

m,n Plate modal indices

List of Figures

List of Tables

Contents

Chapter 1

Introduction

1.1 Motivation

Rectangular ducts are the most commonly used duct geometry in HVAC applications. It is of significant practical interest to predict the noise that transmits through a ducted system from source to a receiver space to achieve a desired noise goal [1]. HVAC systems contain air handling units (AHU) such as fans, blowers and other fluid machinery that act as noise sources. Sound can propagate in different paths from the source (the AHU) to the receiver (the room or space). Figure 1.1 shows the critical sound paths from source to reciever through a ducted system [2]
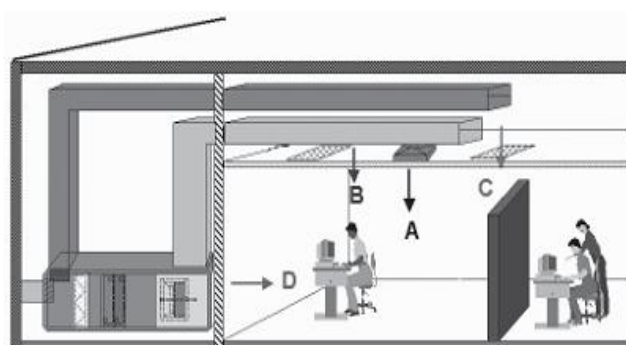
Figure 1.1: Various paths for sound to travel from source to receiver

A. Discharge – sound from the supply air duct. B. Breakout – sound coming through the duct walls (a common problem on poorly designed rooftop systems). C. Return – sound from the return air duct. D. Radiated – sound radiated through the walls of the building.

Other sources that contribute to the noise are the flow induced noise and from other external sources that enter into the duct from outside. In the acoustical design of HVAC systems estimation of noise radiation exterior to the duct is one of the critical parameters. Noise radiation external to the duct due to duct wall vibrations are caused mainly due to hydrodynamic forces and also due to acoustic pressure waves. Noise radiated in the transverse direction from the duct walls is termed as

1

"breakout" noise [3]. Breakout noise is one of the most common paths of sound transmission in HVAC systems for thin wall ducts. The cross section geometry of the duct and thickness play an important role in the breakout noise. Various kinds of commonly used duct cross sections are rectangular, flat oval and circular. Of all the geometries, rectangular ducts have the lowest wall transmission loss at low frequencies. Air – borne and structure borne sounds contribute to duct breakout noise which is more dominant at low frequencies [3]. The physical phenomenon causing breakout noise is the structural - acoustic coupling between the structure and the acoustic domains. Mean flow Mach numbers are negligible in HVAC ducts and so flow effects are not considered in the current work. . The excitation due to hydrodynamic forces generates very low frequency vibration. It might be focus for fatigue analysis. When Acoustic impedance inside the duct is closer to the structural impedance, the acoustic wave excites the structure. The vibration of structure will induce acoustic pressure inside the duct. These phenomena will continue under coupling conditions. Coupling conditions depends on the acoustic and structural natural frequency and spatial distribution of mode shapes. This is termed as called structural-acoustic coupling. Vibration displacement of flexible structure due to acoustic excitation results in sound radiation outside the duct volume. Radiated sound power depends on vibration velocity, surface area and radiation efficiency. Modal radiation efficiencies indicate how efficiently sound power is radiated by a given mode.

So current research is more focused on understanding the sound radiation characteristics from the rectangular duct and also the physical phenomena of structural – acoustic coupling. It has been planned to develop a theoretical model, numerical simulations and experiments. As part of the experimental study, it is planned to do experimental set up for the rectangular duct with one set of boundary conditions and establishing the complete experimental procedure.

1.2 Overview of Literature

Breakout noise from the duct walls is quite an important research area in the field of structural – acoustics. During the past few decades extensive research has been carried out in this area on various duct geometries. The mechanism of duct

breakout noise varies with various duct cross sections. Cummings [3] has provided an overview of complete research work on duct breakout noise that has been carried out for the past two decades. Complete physical phenomenon and the effect of various duct cross section geometries effecting the breakout and break in has been addressed by Cummings [3]. Analytical methods available in literature [3] for sound radiation from the ducts are 1) finite-length line source, 2) equivalent finite–length cylindrical radiator. Methods to reduce the breakout and break in are also reported in reference[3].Allen [4] provided a simple formula for the breakout noise but this is not valid at low frequencies. Cummings [5] described a simple one-dimensional theory for the transverse transmission of low frequency sound through the walls of rectangular ducts. The model is based on a coupled acoustic/structural wave system, and it is assumed that the duct radiates sound in the same way as a finite-length line source. Cummings [5] estimated noise breakout from rectangular duct using line source model and equivalent cylinder model. Cummings [5] has addressed two experimental rigs for structural-acoustics experiments. Experimental set up was made for a rectangular duct and square duct with different acoustic boundary conditions. Cummings and Chang [6] developed two theoretical models for flat oval ducts: first one is based on a numerical solution to the equations of motion for the duct walls, Second model is to determine duct wall response to the internal sound field due to the forced wave acting on the walls for flat-oval ducts. A theoretical treatment of sound transmission through the walls of distorted circular ducts for plane mode transmission has been addressed by Cummings, chang and Astley [7]. Li and Gibeling [8] proposed a near field sound radiation model based on Kirchhoff - Helmholtz Integral formulation by solving quadruple integrals evaluated over a rectangular plate. Kim and Brennan [9] proposed a compact matrix formulation based on impedance- mobility approach for an acoustic-structural coupled problem thereby providing a detailed insight into acoustic – structural systems. In this an experimental set up for a cavity which consisted of five acoustically rigid walls and a simply supported flexible plate on the remaining side is addressed.

Venkatesham et al [10, 11] provided an analytical solution for prediction of breakout noise from rectangular duct and rectangular plenum with four compliant walls based on equivalent plate model for sound radiation. In this model, acoustic pressure and vibration velocity vectors are expressed in terms of uncoupled acoustic and structural sub systems. Sound radiation model leads to quadruple integrals. Venkatesham et al [10, 11] discussed solution procedure of quadruple integrals based on coordinate transformation.

Radiation impedance matrices are function of modal indices. Modal radiation efficiency estimation provides the efficient sound radiation modes in total sound power radiation from a duct. Wallace [12] provided analytical formula for radiation efficiencies at low frequencies from a baffled rectangular plate. The radiation resistance is determined theoretically from the total energy radiated to the far field due to natural modes of a finite rectangular panel. Sound radiation characteristics of box structures studied by Tian Ran, Lin et al [13, 14] provide a basis in understanding the vibrational energy flow between panels of the box, grouping of various modes, their radiation efficiencies and in understanding the kinds of sound sources. Effect of the strong and weak coupling based on transfer factor has been addressed by Louisell [15].W.L.Li [16] proposed an analytical solution for the self and mutual radiation resistances of a simply supported rectangular plate. In this the analytical solution, radiation impedance is represented in the form of a power series in terms of non-dimensional acoustic wave number. Astley and Cummings [17] addressed a finite element scheme and an experimental set up to study the acoustic transmission through the walls of rectangular ducts.

In the current work, analytical model proposed by Venkatesham et al [10, 11] has been implemented to determine the sound radiation characteristics of rectangular ducts. It is assumed that there exists a strong coupling between acoustic-structure interior of the duct and a weak coupling exterior to the duct. Strongly coupled structural modes and acoustic modes are identified based on the transfer factor [15]. The rectangular duct modes are classified into various groups similar to box structures as discussed in reference [13, 14]. Modal radiation efficiencies of different groups of rectangular duct have been estimated and compared analytically

and numerically. Symmetry between the panel pairs and net volume displacements are studied to find out the most efficiently radiating modes. Comparison of the modal radiation efficiencies with that of simple plate provides similarity between duct sound radiation behaviors in terms of plate modes

A numerical study has been conducted based on Finite Element Method and Boundary Element Method with FEM fluid and FEM structure options. Direct Boundary Element Methods (DBEM) method has been adopted to estimate the sound power radiated from the duct walls. The total radiation efficiency due to coupled acoustic modes and coupled structural modes has been calculated. Validation study has been done for the analytical and the numerical data.

An experimental set up for rectangular duct has been designed with structural boundary conditions as simply supported and acoustic boundary conditions as rigid end termination. Acoustical parameters such as total sound power, radiation efficiency, and pressure field measured. Structural parameters such as wall vibration displacement and wall vibration velocity are estimated.

1.3   Outline of Thesis

Chapter 2 discusses the analytical and numerical model of the rectangular duct with validation

Chapter 3 discuss the experimental set up ,fabrication and experimental test procedures for measuring sound power using intensity method, pressure at field point, wall vibration velocity and displacement measurements.

Chapter 4 discusses a comparison of Analytical, Numerical and Experimental data for the selected duct geometry and material properties.

A conclusion for the current work and recommendations for future work are addressed in Chapter 5

Chapter 2

Theoretical Formulation

In this chapter a complete theoretical and numerical model for estimating the total sound power, total radiation efficiency and various other physical parameters has been discussed for one rectangular duct geometry

2.1   Description of Methodology

The flow chart presented below shows an outline of the analytical modeling for the sound radiation from rectangular duct.
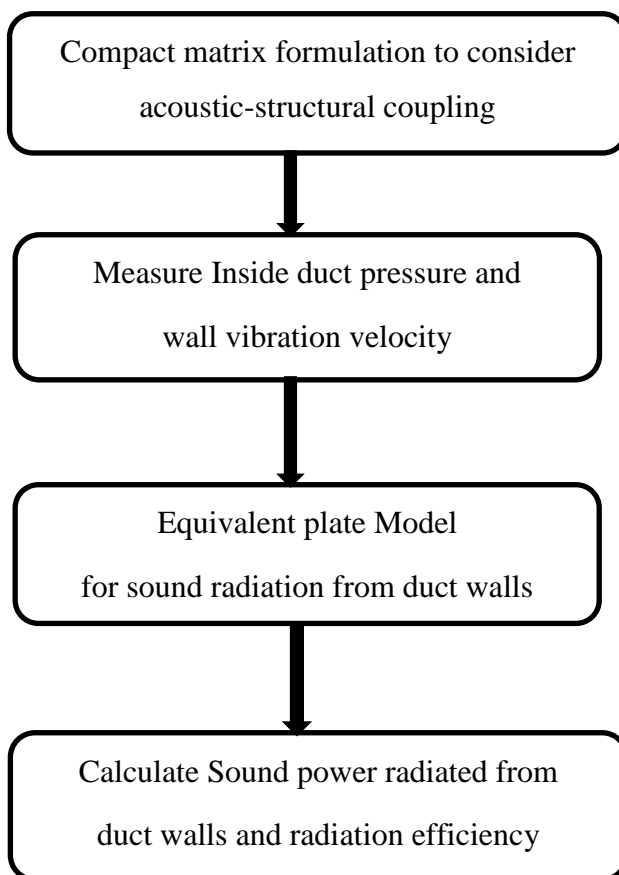
Figure 2.1: Flowchart of theoritical formulation methodology

2.1.1 Compact Matrix formulation

The governing differential equation to determine Sound pressure inside the duct due to acoustic excitation is given by inhomogeneous Helmholtz equation [10].Figure 2.2 shows a schematic representation of the rectangular duct with co-ordinate system [10]. Assumption in this modeling is strong coupling between inside duct volume and flexible duct wall area and weak coupling between flexible wall area and outside environment. Another assumption is coupled behavior can be expressed in terms of finite number of uncoupled acoustic and structural modes.
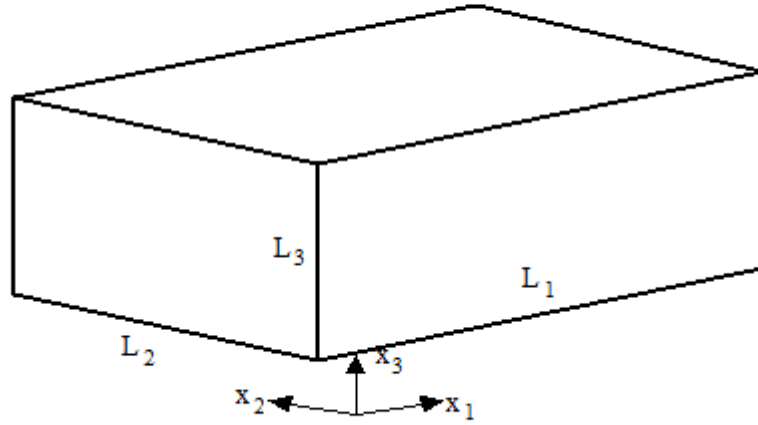
Figure 2.2: Schematic diagram of rectangular Duct

$$(\nabla^2 + k^2)p(\vec{x}) = -j\omega\rho_0 q_{vol}(\vec{x}) \tag{2.1}$$

Subjected to the following boundary condition,

$$\frac{\partial p(\vec{x})}{\partial n} = j\omega\rho_0 u_w \quad \text{On } S_f \tag{2.2}$$

Pressure field inside the duct is given by [10]

$$p(\mathbf{x}, \omega) = \sum_n \Psi_n(\mathbf{x})a_n(\omega) = \mathbf{\Psi}^T \mathbf{a} , \tag{2.3}$$

Where,

$$\Psi_n(\mathbf{x}) = \sum_{n_1 n_2 n_3} \cos\left(\frac{n_1 \pi x_1}{L_1}\right) \cos\left(\frac{n_2 \pi x_2}{L_2}\right) \cos\left(\frac{n_3 \pi x_3}{L_3}\right) \tag{2.4}$$

$$a_n(\omega) = \frac{\rho_0 c_0^2}{V} A_n(\omega) \left[\int_V q_{vol}(\vec{y}) \Psi_n(\vec{y}) \, dV + \int_{S_f} \Psi_n(\vec{y}) u_n(\vec{y}) \, ds \right] \tag{2.5}$$

$$A_n(\omega) = \frac{j\omega}{\omega_n^2 - \omega^2 + 2j\zeta_n \omega_n \omega} \tag{2.6}$$

$$V = \int_V \Psi_n^2(\mathbf{x}) \, dV \tag{2.7}$$

$$q_n = \int_V \Psi_n(\vec{y}) \, q_{vol}(\vec{y}) \, dV \tag{2.8}$$

n_1, n_2, n_3 are acoustical modal indices.

L_1, L_2, L_3 are duct dimensions in x_1, x_2 and x_3 directions respectively.

$\Psi_n(\mathbf{x})$ is the uncoupled acoustic mode shape function.

$a_n(\omega)$ is the complex amplitude of the modal pressure corresponding to the nth acoustic mode.

$A_n(\omega)$ is the acoustic mode resonance term.

q_n is the generalised acoustic source strength for the nth acoustic mode.

ρ_0, c_0 are the density and speed of sound in air.

$u_w(\vec{y})$ is the normal velocity of the compliant duct wall.

V is the duct volume.

$q_{vol}(\vec{y})$ is the fluctuating volume flow per unit volume or the acoustic source strength density function in the cavity volume V.

The governing differential equation for the response of the duct walls due to vibration, subjected to internal pressure and external force on the duct wall is given by [10].

$$D\nabla^4 \xi(\vec{z}) - \rho h \omega^2 \, \xi(\vec{z}) = p(\vec{z}) - f(\vec{z}) \tag{2.9}$$

Where, D is the flexural rigidity given as $\frac{Eh^3}{12(1-v^2)}$ and $\xi(\vec{z})$ represents the normal displacement of the duct walls. Normal deflection of the wall and the normal velocity are related by the relation $u_w(\vec{z}) = j\omega\xi(\vec{z})$. Vibration velocity of the compliant duct walls is estimated based on equivalent plate and is given for axial simple supported boundary conditions [10].

$$u_w(\mathbf{z}, \omega) = \sum_m \Phi_m(\mathbf{z})b_m(\omega) = \mathbf{\Phi}^{\mathrm{T}}\mathbf{b} \tag{2.10}$$

Where,

$$\Phi_m = \sum_{m_1}^{p_s}\sum_{m_2}^{q_s} A_{m_1,m_2} \sin\left(\frac{m_1\pi x}{L}\right)\sin\left(\frac{m_2\pi x_1}{L_1}\right) \tag{2.11}$$

$$b_m(\omega) = \frac{1}{\rho_s h S_f} B_m(\omega)\left(\int_{S_f}\Phi_m(\mathbf{z},\omega)f(\mathbf{z},\omega)\,dS - \int_{S_f}\Phi_m(\mathbf{z},\omega)p(\mathbf{z},\omega)\,dS\right)$$

$$\tag{2.12}$$

$$B_m(\omega) = \frac{j\omega}{\omega_m^2 - \omega^2 + j2\zeta_m\omega_m\omega} \tag{2.13}$$

$$\mathrm{g}_m = \int_{S_f}\phi_m(z)f(z,\omega)\,dS \tag{2.14}$$

$$S_f = \int_{S_f}\Phi_m^2\,dS \tag{2.15}$$

Φ_m is the uncoupled structural mode shape function.

b_m is the Complex amplitude of the mth vibration velocity mode.

$B_m(\omega)$ is the structural mode resonance term.

g_m is the generalised modal force vector.

ρ_s is the density of the duct wall material.

h is the thickness of the duct wall.

S_f is the Surface area of the wall.

m_1, m_2 are the modal indices along x and x_1 of the plate.

A_{m_1,m_2} is the Eigen expansion function.

Equations (2.5) and (2.12) can be further simplified as [9]

$$a_n = \frac{\rho_0 c_0^2}{V} A_n(\omega)\left[q_n + \sum_{m=1}^{M} C_{n,m} b_m(\omega)\right] \tag{2.16}$$

$$b_m(\omega) = \frac{1}{\rho_s h S_f} B_m(\omega)\left(g_m - \sum_{n=1}^{N} C_{n,m}^T a_n(\omega)\right) \tag{2.17}$$

$$C_{n,m} = \int_{S_f} \Psi_n(\bar{y}) \Phi_m(\bar{y})\ dS \tag{2.18}$$

The coupled response between the structural and acoustic domains is represented in the form of uncoupled acoustic and structural subsystems using impedance-mobility approach [10]. Modal acoustic pressure vector defined in Equation 2.16 interms of impedance & mobility is given as

$$\mathbf{a} = \mathbf{Z_a}(\mathbf{q} + \mathbf{q_s}) \tag{2.19}$$

$\mathbf{Z_a} = \frac{A \rho_0 c_0^2}{V}$ is the Uncoupled acoustic modal impedance matrix and $\mathbf{q}$ is the modal source strength vector and $\mathbf{q_s} = \mathbf{Cb}$ Where $\mathbf{C}$ is matrix representing coupling coefficient $C_{n,m}$ between n[th] acoustic mode and m[th] structural mode. Coupling represents the spatial distribution of acoustic mode on flexible surface and matching of uncoupled acoustic and structural natural frequencies. Modal structural vibration defined in Equation 2.17 interms of impedance and mobility velocity vector is given by

$$\mathbf{b} = \mathbf{Y_s}(\mathbf{g} - \mathbf{g_a}) \tag{2.20}$$

$\mathbf{Y_s} = \frac{B}{\rho_s h S_f}$ represents uncoupled structural modal mobility matrix and $\mathbf{g}$ is the generalized modal force vector and $\mathbf{g_a} = \mathbf{C^T a}$

Using Equations (2.19) and (2.20)

$$\mathbf{a} = (1 + \mathbf{Z_a C Y_s C^T})^{-1} \mathbf{Z_a}\ (\mathbf{q} + \mathbf{C Y_s g}) \tag{2.21}$$

$$\mathbf{b} = (\mathbf{1} + \mathbf{Y_s C^T Z_a C})^{-1} \mathbf{Y_s} \, (\mathbf{g} - \mathbf{C^T Z_a q}) \tag{2.22}$$

2.1.2 Pressure field inside the duct and wall vibration velocity

Pressure field inside the duct is given by [11]

$$p(\mathbf{x}, \omega) = \sum_n \Psi_n(\mathbf{x}) a_n(\omega) = \mathbf{\Psi}^T \mathbf{a} \tag{2.23}$$

Vibration velocity of the compliant duct walls is estimated based on equivalent plate presentation model and is given as the following for axial simple supported boundary conditions [11]

$$u_w(\mathbf{z}, \omega) = \sum_m \Phi_m(\mathbf{z}) b_m(\omega) = \mathbf{\Phi}^T \mathbf{b} \tag{2.24}$$

2.1.3 Equivalent plate representation

The duct mode shapes and natural frequencies are calculated by using Rayleigh –Ritz method [18]. In this method unfolded equivalent plate representation is used to model the rectangular duct. The folded boundary is modeled as rotational spring and at creases of two adjacent plate panels as linear springs. A simply supported boundary condition along the axial directions is then applied to the equivalent plate boundaries. Figure 2.3 shows the equivalent plate representation.
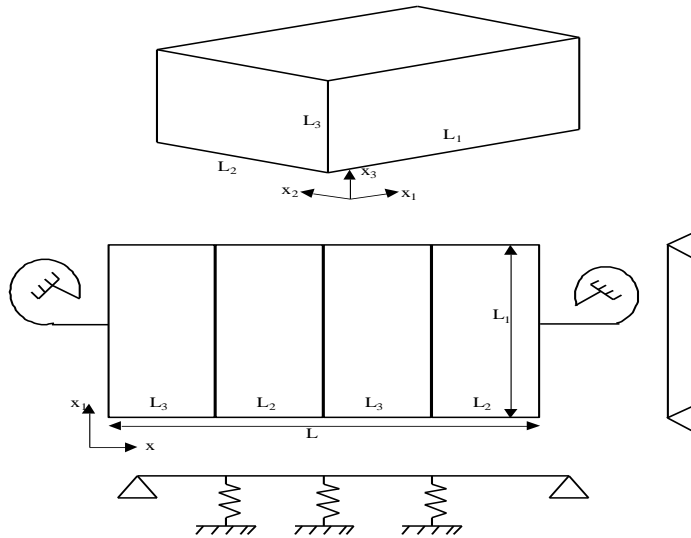
Figure 2.3: Equivalent plate representation of rectangular duct with simply supported boundary condition.

11

The details of Rayleigh-Ritz model of equivalent plate to calculate uncoupled natural frequency for various axial boundary conditions is given in [19].

Furher details are given in Appendix A

Net volume displacement for each mode is calculated using the formula

$$v_{net} = \sum_{n=1}^{4} (\sum_m \Delta v_m)_n \qquad (2.25)$$

Where

n represents the panel number varying from 1 to 4 which are considered as the four walls of the duct.

v_{net} represents the net volume displacement for a given mode.

Δv_m is the volume displacement associated with the amplitude displacement of the mth elements in an nth plate panel i.e. each duct wall [13].

Sound power radiation from the equivalent plate model is calculated using Rayleigh integral method [10]. Quadraple integrals are involved in the calculation of sound power radiation.These are converted to double integrals and finally to single integrals using coordinate transformation [10, 11].

2.1.4 Calculation of Sound power and Radiation efficiency

Sound power radiation from a baffled plate in terms of modal amplitudes of vibration velocity and radiation impedance matrix is given as [10, 11]

$$W_{rad} = \frac{1}{2} \mathbf{b^H} Re[\mathbf{Z}] \mathbf{b} \qquad (2.26)$$

$$Re\left[Z_{m_1 m_2 m_1' m_2'}\right] = \frac{k}{2\pi} \int_0^L \int_0^{L_1} \int_0^L \int_0^{L_1} \sum_{m_1} \sum_{m_2} A_{m_1 m_2} \sin\frac{m_1 \pi x}{L} \sin\frac{m_2 \pi x_1}{L_t} * \dots$$

$$\sum_{m_1'} \sum_{m_2'} A_{m_1' m_2'} \sin\frac{m_1' \pi x'}{L} \sin\frac{m_2' \pi x_1'}{L_1} \frac{\sin kR}{R} dx_1' \, dx' \, dx_1 \, dx \qquad (2.27)$$

Where,

$$R = \sqrt{(x - x')^2 + (x - x_1')^2} \qquad (2.28)$$

$$Re\left[Z_{m_1 m_2 m_1' m_2'}\right] = \frac{k}{2\pi} \sum_{m_1} \sum_{m_2} \sum_{m_1'} \sum_{m_2'} A_{m_1 m_2} A_{m_1' m_2'} I_{m_1 m_2 m_1' m_2'} \qquad (2.29)$$

$$I_{m_1 m_2 m_1' m_2'} = \int\limits_0^L \int\limits_0^{L_1} \int\limits_0^L \int\limits_0^{L_1} \sin\frac{m_1 \pi x}{L} \sin\frac{m_2 \pi x_1}{L_1}$$

$$\sin\frac{m_1' \pi x'}{L} \sin\frac{m_2' \pi x_1'}{L_1} \frac{\sin kR}{R} \, dx_1' \, dx' \, dx_1 \, dx \qquad \textbf{(2.30)}$$

Simplification of Integral in Equation (2.30) is given in Appendix B

Modal Radiation efficiency as a function of frequency is calculated as [14]

$$\sigma = \frac{W_{rad}}{W_{in}} \qquad \textbf{(2.31)}$$

W_{rad} is the radiated sound power   and W_{in} is the sound power radiated by a piston source having the same surface area of the structure and vibrating with the same root mean square velocity [14] S_f is the flexible wall area and is given by $L \times L_1$. Vibration velocity of the structure is calculated using Equation 2.29

$$W_{in} = \rho_0 c_0 S_f \langle \mathbf{b} \rangle^2 \qquad \textbf{(2.32)}$$

Identification of the strongly coupled acoustic modes and structural modes is based on the calculation of the transfer factor [15] which is defined as follows

$$T_{n,m} = \left(1 + \frac{(\omega_n^2 - \omega_m^2)\rho_s h S_f V}{4\rho_0 c_0^2 C_{n,m}^2} \right)^{-1} \qquad \textbf{(2.33)}$$

$T_{n,m}$ corresponds to n^{th} acoustic mode coupled to m^{th} structural mode respectively.

2.1.5   Calculation of Plate radiation efficiency

Modal radiation efficiency for simply supported rectangular plate can be calculated   by using the following analytical equations [12].Below equations are valid for ka and $kb \ll 1$

$$\sigma_{mn} = \frac{32k^2 ab}{m^2 n^2 \Pi^5} \left\{ 1 - \frac{k^2 ab}{12} \left[\left(1 - \frac{8}{m^2 \Pi^2} \right)\frac{a}{b} + \left(1 - \frac{8}{n^2 \Pi^2} \right)\frac{b}{a} \right] \right\} + \text{o}\,(k^6) \qquad \textbf{(2.34)}$$

$$\sigma_{mn} = \frac{8k^4 ab^3}{3m^2 n^2 \Pi^5} \left\{ 1 - \frac{k^2 ab}{20} \left[\left(1 - \frac{8}{m^2 \Pi^2} \right)\frac{a}{b} + \left(1 - \frac{24}{n^2 \Pi^2} \right)\frac{b}{a} \right] \right\} + \text{o}\,(k^8) \qquad \textbf{(2.35)}$$

$$\sigma_{mn} = \frac{2k^6 a^3 b^3}{15m^2 n^2 \Pi^5} \left\{ 1 - \frac{k^2 ab}{28} \left[\left(1 - \frac{24}{m^2 \Pi^2} \right)\frac{a}{b} + \left(1 - \frac{24}{n^2 \Pi^2} \right)\frac{b}{a} \right] \right\} + \text{o}\,(k^{10}) \qquad \textbf{(2.36)}$$

13

The terms in the above equations can be further expanded based on the equations in [16].

Cut off frequency for the simply supported rectangular plate can be calculated

Using the formula [12]

$$\omega_c = c_0 \left[\left(\frac{m\pi}{a}\right)^2 + \left(\frac{n\pi}{b}\right)^2 \right]^{1/2} \tag{2.37}$$

2.2 Numerical Model

A numerical model based on FEM structure and FEM fluid is developed and linked them for coupled analysis. Below flow chart gives an outline of the numerical modeling procedure to calculate sound power radiation and radiation efficiency.
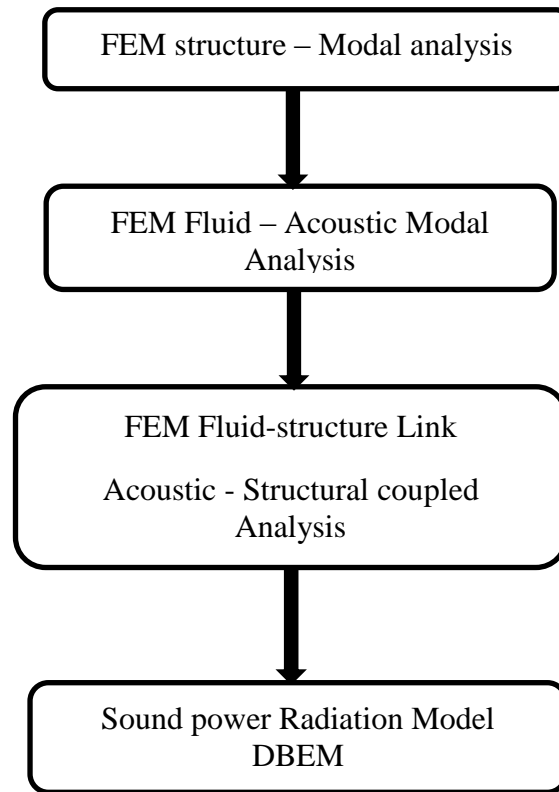
Figure 2.4: Flow Chart of Numerical Model

2.2.1 FEM-Structure

A rectangular duct of dimensions 0.3 m x 0.4 m x 1.5 m ($L_1 = 1.5, L_2 = 0.3, L_3 = 0.4$) with a thickness of duct wall 5 mm is modeled and meshed using

SHELL 63 elements[20]. Structural boundary condition in the form of simply supported boundary condition is applied. An element size of 0.01 is given for the model based on convergence study. Total number of elements in the model is 21000.

Material properties of aluminum are applied to the structure that are given as $\rho_s = 2770$ kg/m^3, Young's modulus E $=$ 71 Gpa, Poisson's ratio $\upsilon = 0.33$, and structural damping ratio $= 0.01$,

Figure 2.5a and Figure 2.5b shows the schematic and the meshed model of the structure.
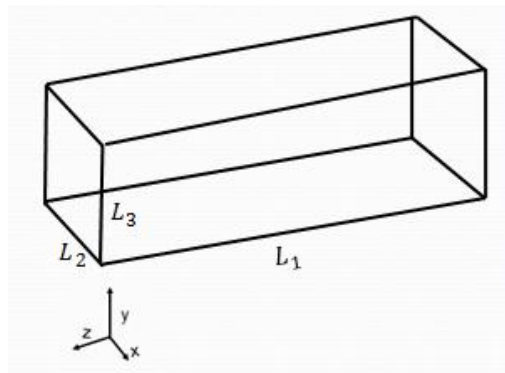
Figure 2.5a: Schematic diagram of rectangular duct
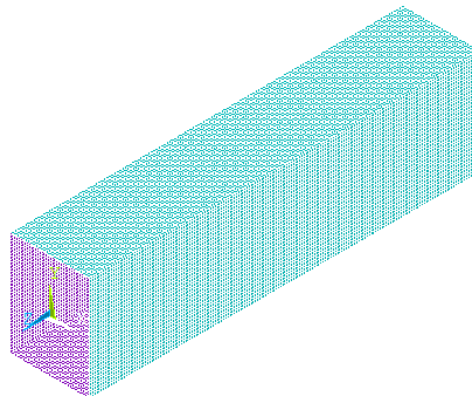
Figure 2.5b: Meshed model of rectangular duct

2.2.2 Description of Acoustic Model

The enclosed duct volume of dimensions 0.3m x 0.4m x 1.5m is modeled and meshed using SOLID185 elements [20]. Acoustically rigid end terminal boundary conditions are applied. The maximum element size is chosen such away that it should satisfy six elements for wavelength criteria. Number of divisions along the x, y, z are 30, 40,120 chosen for meshing. Total number of elements is 180000.

Air properties are applied to the acoustic volume with c_0=340 m/s, $\rho_0 = 1.225$ kg/m^3, Acoustic damping ratio = 0.01, Rigid terminal impedance as $z_t \rightarrow \infty$ or admittance is zero.

Figure 2.6a and Figure 2.6b shows the schematic and the meshed model of the acoustic domain.
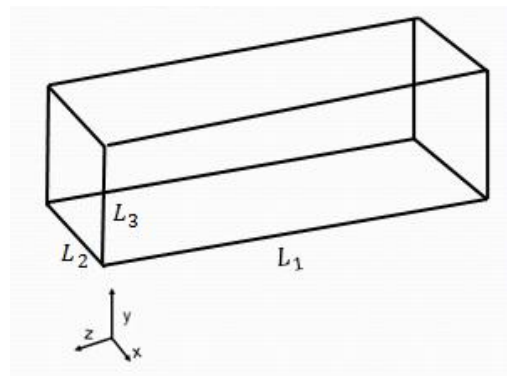
Figure 2.6a: Schematic diagram of the volume enclosed by the duct
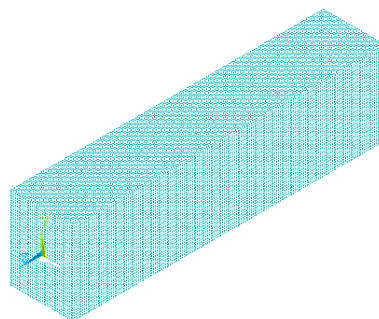
Figure 2.6b: Meshed model of the acoustic Volume

2.2.3 Description of Coupled Model

The problem of acoustic-structure interaction involving structural (duct) and acoustic (volume inside the duct) domains has been solved in FEM acoustic module in LMS virtual lab [21].The first step in the current model is importing acoustic and the structural models into a single file and link them to do solve a vibro - acoustic analysis. Acoustic excitation in the form of a constant velocity piston source is provided by giving a constant velocity input at inlet face of the acoustic mesh. This analysis solves a coupled system of equations to determine the structural displacements on the duct walls and the pressure inside the duct by coupling structure and acoustic models with acoustic excitation.

Figure 2.7a and Figure 2.7b show the schematic and the meshed model of the Acoustic-structure model
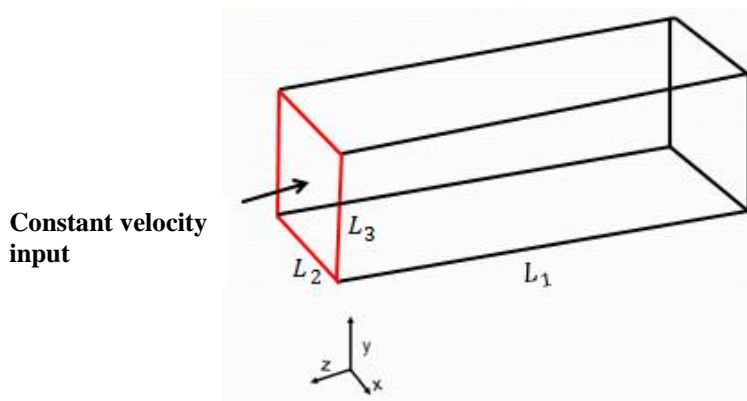
Figure 2.7a: Schematic diagram of the acoustic - structural model
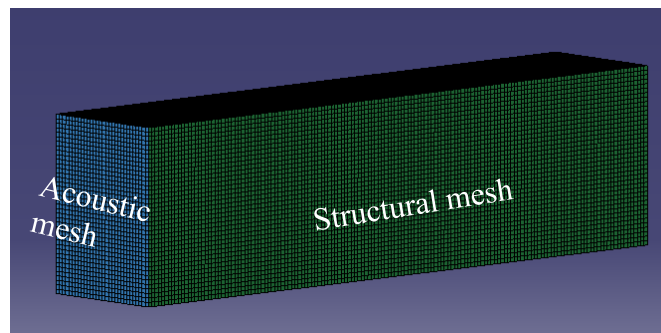
Figure 2.7b: Meshed model of the acoustic-structural coupled model

2.2.4 Description of Sound radiation model

The total sound power radiated from the duct walls is estimated using Direct Boundary element method (DBEM) option of BEM acoustics and also considered exterior sound radiation problem. A three-dimensional acoustic radiation analysis requires a 2D mesh of the sound radiating surface. In the present case it is the 2D mesh of the duct walls. Mesh coarsening is done from a finely defined FE mesh to a coarser BE acoustic mesh. The minimum element edge size should satisfy at least six elements per wavelength which is a rule of thumb. In the present work the studies are valid till 400 Hz so the element edge size is given by $\lambda/6 = c/(6 \times 400)$ =0.1.So an element size of 0.02 is used to get better converged results.

In the first step of BEM, acoustic potentials – pressure and particle velocity are solved on the BE mesh. In order to determine the sound radiated to the exterior of the duct, acoustic potentials are solved on the field point mesh which is a virtual surface surrounding the BE mesh. It is assumed that the field point mesh is a nonreflecting surface where the wave just propagates and doesn't reflect. Figure 2.8 shows the BE mesh and the fold point mesh. The dimensions of the field point mesh are 0.4m x 0.5m x 1.5m
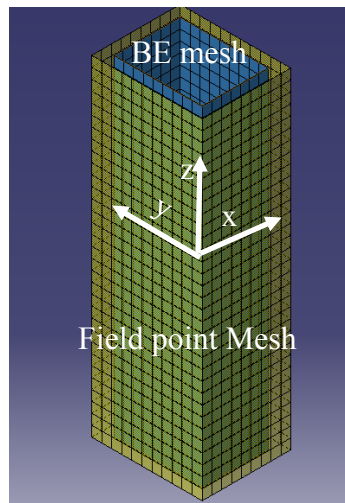
Figure 2.8: BE mesh and field point mesh

Sound radiation problem solves for total acoustic power radiated by the structure, total radiation efficiency, input power and mean quadratic velocity

From mean quadratic velocity volume velocity can be estimated by taking the square root of mean quadratic velocity and then multiplying with the duct wall area.

Modal radiation efficiency is estimated numerically by activating the selected structural or acoustic modes. The selection of these modes is obtained by identifying the structural and acoustic modes with identical natural frequencies.

A single acoustic mode can be coupled to multiple structural modes to estimate radiation efficiency and vice versa.

Chapter 3
Experimental setup & Test Procedures

This chapter describes the complete experimental set up for measuring sound radiation charecteristics of a rectangular duct subjected to simply supported boundary conditions. Various measurement procedures to determine structural and acoustic parameters have been reported.

3.1   Experimental set up

A rectangular duct of 0.3 m wide 0.4 m height and 1.2 m length with 20 gauge (1.01 mm) is considered for experimental study. These dimensions have been chosen based on the standard sizes of ducts used in HVAC applications. Figure 3.1a shows the CAD model of the rectangular duct. Figure 3.1b shows the Schematic diagram of the rectangular duct with all the dimensions in mm.
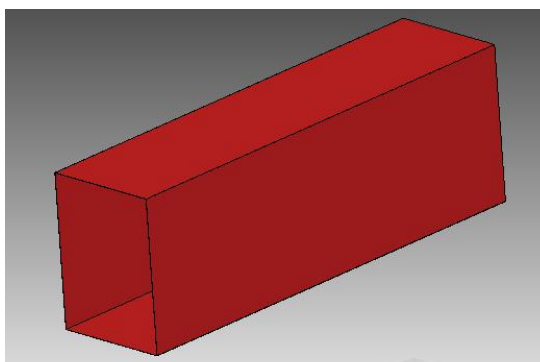
Figure 3.1a: CAD model of rectangular duct
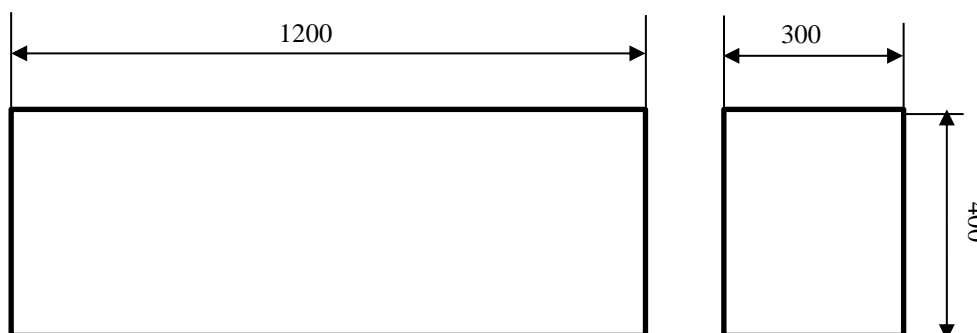
Figure 3.1b: Schematic diagram of rectangular duct

Galvanized Iron (GI) sheet of 1.4 m width and 1.2 m length is bent to specified dimensions. The ends of the sheet are jointed properly in longitudinal direction so that there is no sound leakage to the exterior.

Front side of the duct is covered by a mild steel plate of 3 mm thickness. A hole diameter of Ø122 mm is provided on the front plate to mount the speaker. To provide a rigid acoustic boundary condition a back plate of 3 mm thickness is mounted on the back side of the duct. This kind of arrangement is made to create a strong standing wave inside the duct. Figure 3.2a shows the front plate and the back plate of the duct. Figure 3.2b shows the two-dimensional model of the front plate and back plates.
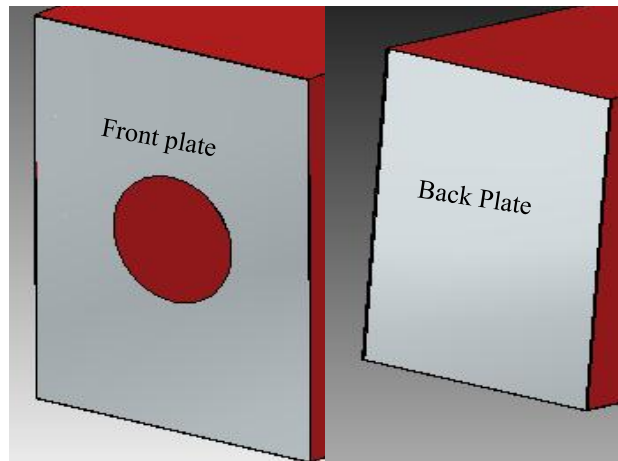
Figure 3.2a: Front plate and back plate of the duct
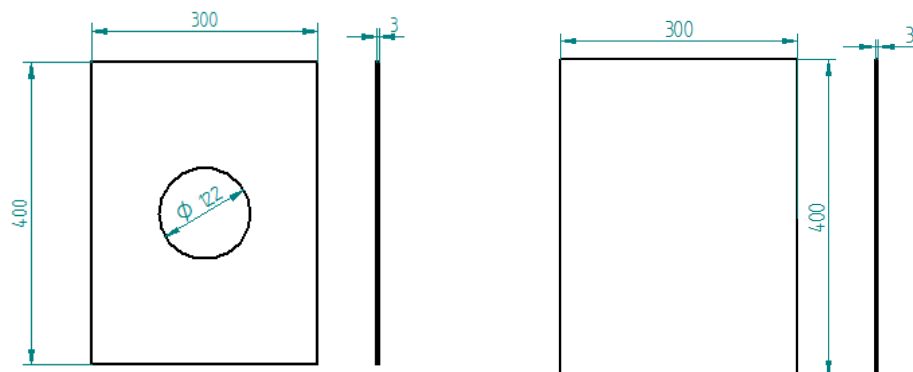
Figure 3.2b: Two dimensional views of the front and back plate

Since the speaker and the support mountings cannot be placed at the same location an extra length of 100 mm each on either sides of the duct is provided in order to ensure proper mounting of the supports. This extra length for supports is fabricated by using a mild steel sheet of higher thickness of 1.4 mm compared to duct wall thickness.

Figure 3.3 shows the fabricated duct with front plate, end plate and extra support length.
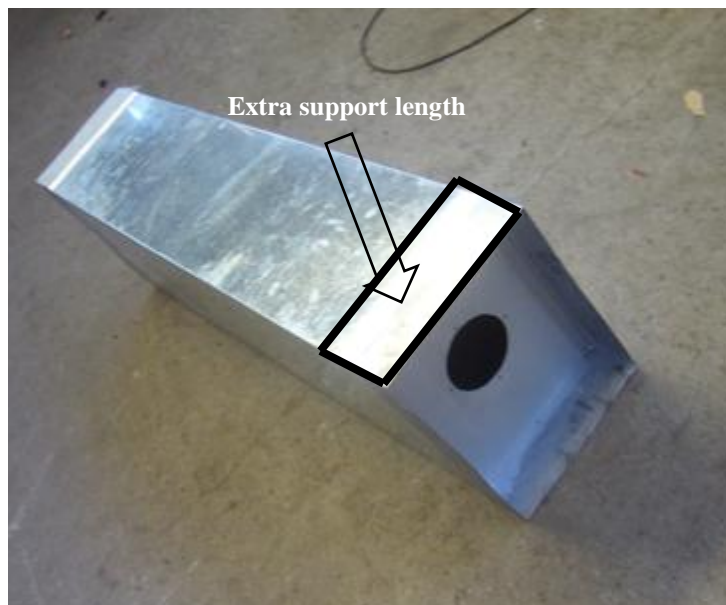
Figure 3.3: Duct with front plate, end plate and extra support length

A simply supported boundary condition is established on the either sides of the duct over the extra support portion. This kind of arrangement is established by providing a custom made rectangular bearing arrangement on either side of the duct. Figure 3.4a shows the CAD model of simply supported boundary set up on the duct, a detail view of the balls in point contact with the duct is shown on right side of Figure 3.4b shows the two-dimensional (2D) view with the entire dimension in mm.Figure 3.4c shows the fabricated simply supported frame with steel balls in point contact.
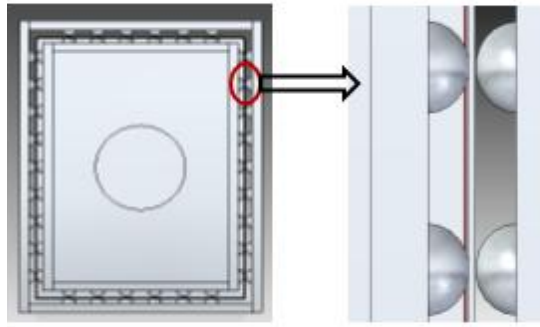
Figure 3.4a: Simply supported boundary condition fixture and detail view of balls in point
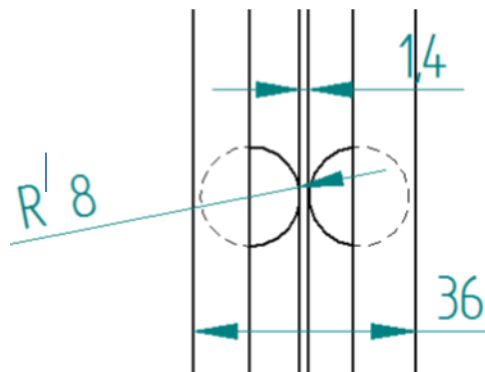
Figure 3.4b: 2D View of the balls in point contact with the duct support

Figure 3.4c: Simply-Supported frame with steel balls in point contact

23

The entire set up is supported by the fixture assembly. The fixture assembly consists of a top plate and bottom plate with the simply supported rectangular frame fit in between them. The top and bottom plates are supported by a hook kind of fixture with blocks attached to the fixture. Figure 3.5a shows the CAD model of fixture assembly. Figure 3.5b shows the 2D model of the assembly with all dimensions in mm.Figure 3.5c shows the fabricated fixture assembly.
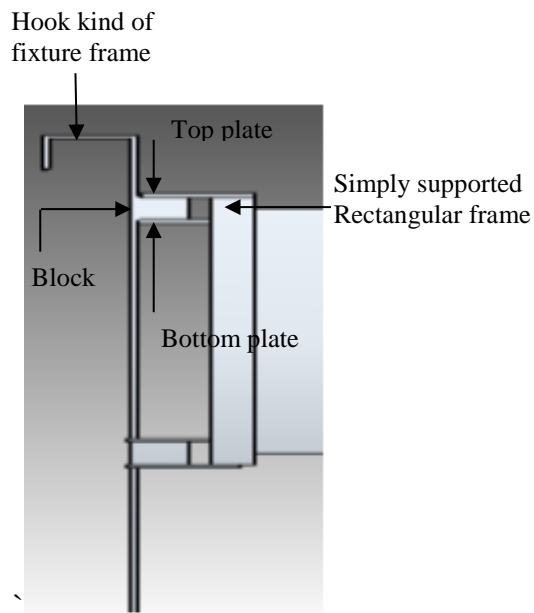
Figure 3.5a: CAD model of the fixture assembly in front view
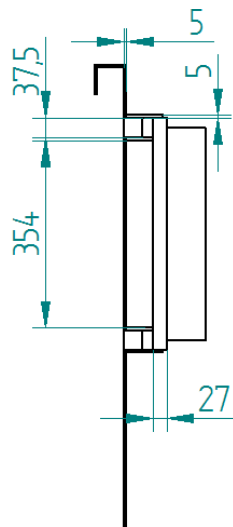
Figure 3.5b: 2D View of the fixture assembly with dimensions

Figure 3.5c: Fabricated fixture assembly

A rectangular grid is created surrounding the four walls of the duct. This grid set up is required to conduct sound intensity measurements. Details of this are given in section 3.3.3.Figure 3.6 shows the complete experimental set up.

Figure 3.6: Experimental set up

An enclosure is designed to avoid any sound leakage from the back side of the speaker .The enclosure is made of plywood with dimensions 230mm x 240mm and 8 mm thickness is provided. Inner walls of the enclosure are covered with two layers of absorptive material of 20 mm thickness with acoustic foam panel of 10 mm and fiber glass 10 mm thickness. This kind of arrangement is done to ensure for

better absorption of the sound leakage in the back side of the speaker..A rubber isolator is glued with adhesive on enclosure edges to avoid vibrations transfer from the speaker to duct.Figure 3.7 shows enclosure with absorptive material on the inner walls.

Figure 3.7: Enclosure with absorptive material on the inner walls and isolator on enclosure edges.

3.2 Instrumentation

The instrumentation used for experimental studies consists of

- ✓ Speaker
- ✓ Data Acquisition systems(DAQ System)
- ✓ Amplifier
- ✓ B & K sound level meter with ½" microphone
- ✓ B & K sound intensity measurement kit.
- ✓ Accelerometer
- ✓ ¼" Microphone

3.2.1 Speaker

Speaker is used for providing acoustic excitation. It is a high quality full range ceiling speaker of model CS-5061T manufactured by AHUJA speaker solutions. The speaker is provided with various power taps of 6W/3W/1.5W on 100 V line matching transformer. It has a 5 inch diaphragm with a frequency response of 60 Hz -15000 Hz. Sound pressure level for the speaker measured at 1 meter distance for an input power of 1 W is given as 92 dB. Figure 3.8a shows the speaker and Figure 3.8b shows the speaker transformer diagram.

Figure 3.8a: Speaker

Figure 3.8b: Speaker transformer with power tapping

Every speaker has a characteristic called directivity which is defined as the directional measure of any sound source. Directivity measurements are done for the

speaker to know its directional characteristics. Measurements are carried out in the semi-anechoic chamber and measurements are taken with the help of B&K Sound level meter. Microphone Type 4189 is used with the analyzer to record the pressure data. Sound level meter is placed at 1 m from the speaker being tested, and at the same height as that of the center of the speaker. Speaker is placed on a table and rotated every 30^0. The setup is not disturbed till the measurement procedure is completed. Input is given to the speaker in the form of a sine signal at two frequencies at 250 Hz, 500 Hz and a pink noise excitation. Figure 3.9a -3.9c shows the speaker directivity curves at two sine frequencies measured at 250 Hz, 500 Hz and pink noise.
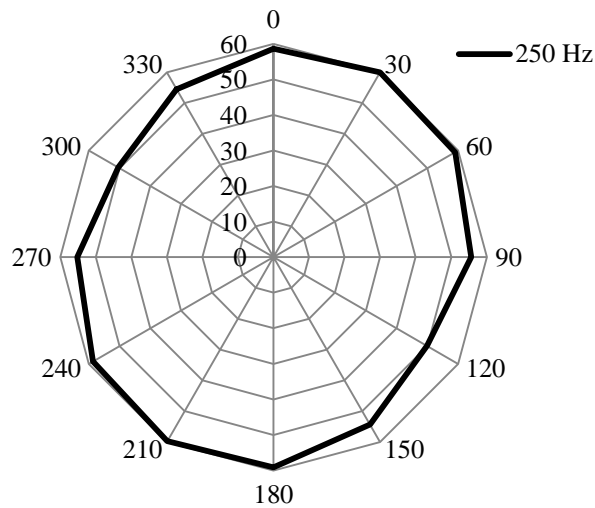
Figure 3.9a: Directivity curve at 250Hz
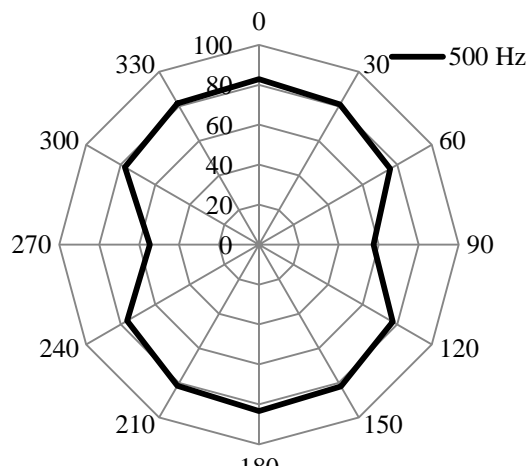
Figure 3.9b: Directivity curve at 500Hz

28
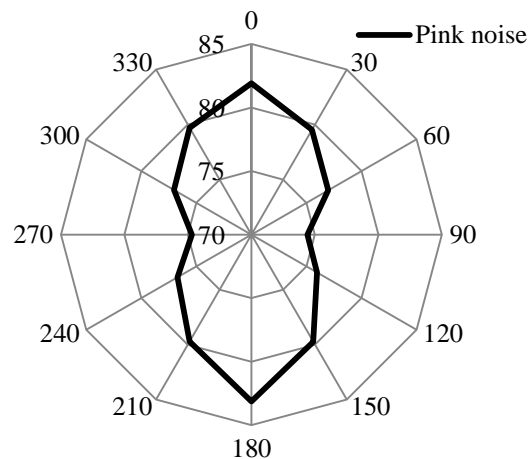
Figure 3.9c: Directivity curve at Pink noise

Figure 3.9a shows the directivity of speaker at 250 Hz each concentric ring of the curve represents a 10 dB change in sound pressure level. Figure 3.9b shows the directivity of speaker at 500 Hz and each concentric ring in the graph represents a 20 dB sound pressure level change. Figure 3.9c each concentric ring in the graph indicates a 5 dB sound pressure level change. From the Figures 3.9a-3.9c it can be observed that speaker radiates more sound at 0^0 and 180^0 compared to all other directions.

3.2.2 Data Acquisition systems(DAQ System)

Data acquisition is the process of sampling signals that measure real world physical conditions and converting the resulting samples into digital numeric values that can be manipulated by a computer..Two DAQ's are used in the experiments. SO analyzer by *m+p International* and PHOTON+ with RT Pro software from *B & K* .Figure 3.10a and Figure 3.10b show the DAQ's used in the current study. PHOTON+ [22] has been used to generate the output waveform which is given as input to the speaker as excitation. SO analyzer is used to record the pressure and acceleration data while conducting acoustic and vibration measurements [23]

Figure 3.10a: SO Analyzer

Figure 3.10b: PHOTON+

3.2.3   Amplifier

Amplifier is used to increase the power of the input signal coming from the output of the DAQ before sending to the speaker. Amplifier of model SWA 100 from BSWA is used. A knob is provided for gain control which is used to adjust the output to the speaker. Figure 3.11 shows the amplifier

Figure 3.11: Amplifier

3.2.4 B & K sound level meter 2270

This is an advanced, dual-channel, hand-held analyzer and sound level meter which is used to perform high-precision, Class 1 measurement tasks in environmental, occupational and industrial application areas [24].This sound level meter is used along with ½ " microphone free field polarized microphone of model number 4189. Figure 3.12[24] shows the hand held analyzer with the microphone.

Figure 3.12: B& K Hand held Analyzer with Microphone

3.2.5 B & K Sound Intensity measurement kit

Sound intensity measurement is done using sound intensity measurement set up from B & K Sound intensity measurement set up consists of ½ "

microphone pair   connected to a preamplifier. Part 1 of the microphone pair is connected to cable A of the preamplifier and part B of the microphone pair is connected to the cable B.A spacer is connected between the microphone pair to [25] to maintain constant distance between the microphones. Figure 3.13 shows the microphone pair, spacer with preamplifier

Figure 3.13: Microphone pair with spacer

Three different sizes of spacer 6mm, 12mm and 50mm are provided. The choice of the spacer to be selected depends on the frequency range of interest. In the present study a spacer of 50 mm is selected whose effective frequency range is from 63 Hz - 1250 Hz. An extension stem is provided for holding the probe. The probe can be rotated conveniently so that it is always oriented normal to the measuring surface. Figure 3.14 [25] shows the complete sound intensity measurement kit.

Figure 3.14: Sound Intensity Measurement set up

3.2.6 Accelerometer

Vibration measurements are done by using accelerometer for estimating structural parameters such as wall vibration velocity and wall displacement. Accelerometer used is from Dytran instruments, INC with model number 3055B3 and serial number 142B2.The sensitivity of the accelerometer is 503.96 mV/g. Figure 3.15 shows the accelerometer.

Figure 3.15: Accelerometer

3.2.7 Microphone

A ¼" free field microphone is used for measuring the acoustic pressure on the field point mesh. Microphone used is provided by PCB which is of model number 378C01 with a sensitivity of 2.37 mV/Pa.Figure 3.16 shows the ¼" microphone

Figure 3.16: 1/4 "Microphone

3.3 Experimental Procedures

The following are various experiments conducted to measure acoustic and structural parameters.

- Vibration measurement
- Acoustic pressure measurement
- Sound intensity measurement

3.3.1 Vibration measurement

Vibration measurement is done for estimating displacement of the duct walls and the wall vibration velocity due to acoustic excitation.

3.3.1.1 Displacement measurement.

Measurements are taken by mounting the accelerometer on the duct wall at the mid cross - sectional plane of the duct. Twenty points are taken along the cross section and at each point ten averages are taken to measure the data. The acceleration data is then converted to displacement by dividing with ω^2 by assuming vibration measurement behavior is time harmonic in nature.

Schematic of the test set up used for measurement is shown in Figure 3.17a & b shows the accelerometer mounted on the duct for measurement.
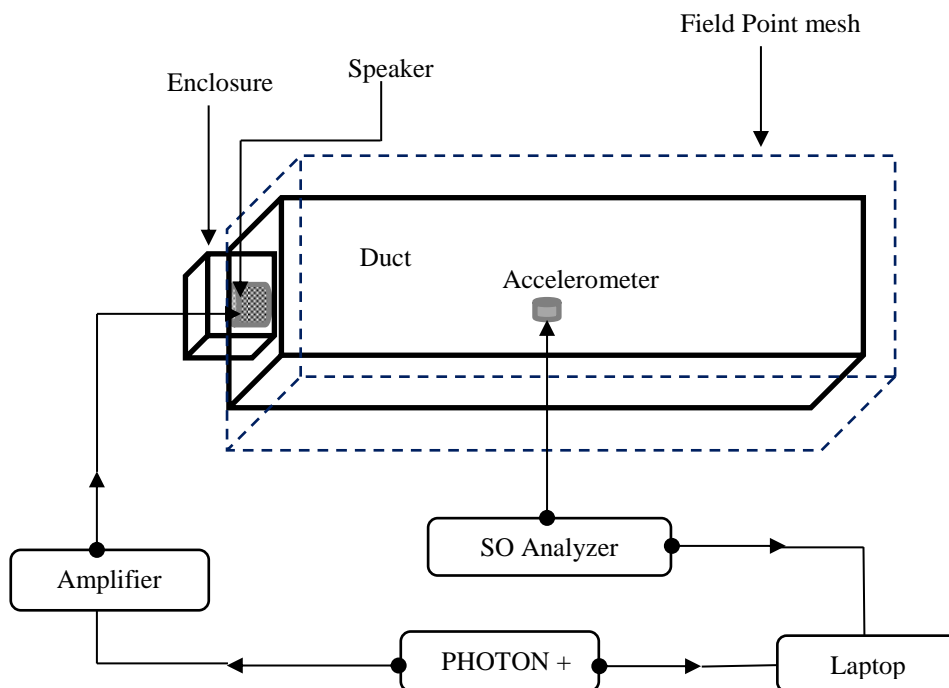
Figure 3.17a: Schematic diagram of the test set up

Figure 3.17b: Accelerometer mounted on the duct

3.3.1.2 Vibration Velocity Measurement

Wall Vibration velocity measurement is done to determine the radiation efficiency. Radiation efficiency can be determined approximately in experiments by measuring the mean square velocity at a number of discrete points on the surface [26]

$$\langle \overline{v^2} \rangle \approx \left(1/N \right) \sum_{i=1}^{N} \overline{v_i^2} \tag{3.1}$$

Where N is the number of measurement points on the surface.

$\langle \overline{v^2} \rangle$ represents space –averaged mean square vibration velocity.

Below is the procedure for calculating the space –averaged mean square vibration velocity

- Measurements are taken at 165 points on the duct walls to get RMS vibration velocity as a function of frequency on the duct.
- Square of the RMS value at each point value is calculated to find out the square of spatial average.

35

- Mean values of all points is then taken to find the spatial average.

Radiation efficiency can be calculated after finding $\langle \overline{v^2} \rangle$ using Equation 2.31.

3.3.2 Pressure measurement

Pressure measurements are taken on the field point mesh at the mid cross - sectional plane of the duct. Measurements are taken by holding the microphone close to every grid point along the cross sectional plane.

Schematic of the test set up used for measurement is shown in Figure 3.18a and Figure 3.18b shows the microphone held over the grid point for measurement
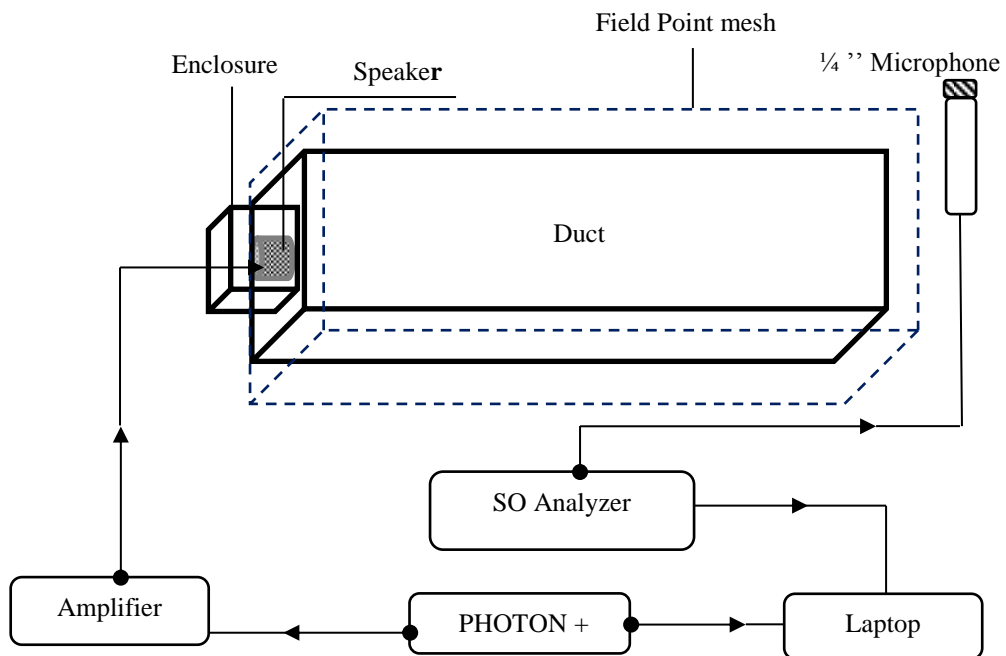
Figure 3.18a: Schematic diagram of the test set up
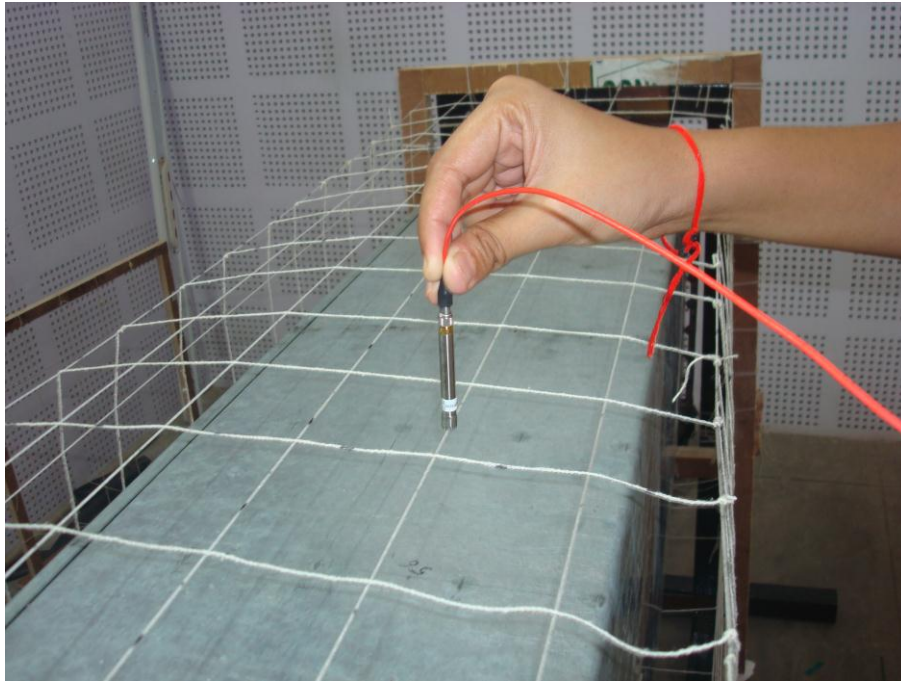
Figure 3.18b: Microphone held at the grid point for pressure measurement

3.3.3   Sound Intensity Measurement

Sound Intensity measurement is used to determine the total sound power radiated from the duct walls. Various standards used for measurement of sound intensity are ISO-9614/1-1993, ISO 9614/2-1996 and ISO 9614/3-2002.In all this methods the acoustic intensity is measured over an imaginary surface surrounding the sound radiating surface.

A discrete - point sampling method is used in ISO 9614-1 to measure the intensity field normal to the measurement surface. Scanning based approach is used in ISO 9614-2 and ISO 9614-3 to measure the normal intensity over the measurement surface.

All this methods help in determining the total acoustic power radiated by the source and also the acoustic energy flow at any point in the space. It also helps in identifying noise source. In order to measure the intensity, a test surface which encloses the sound source is set up. The intensity probe is then used to scan over the created test surface.

Sound intensity over the test surface can be determined either by taking measurements at discrete points on the test surface or by scanning over the test surface. Sound power is then determined as

$$W = I_n S \qquad (3.2)$$

Where W is the total power radiated by the source.

I_n is the intensity normal to the surface

S is the surface area of the test surface

3.3.3.1 Creating Test surface

The first step in doing sound intensity measurement is to create a scanned surface surrounding surface the test surface. The scanned surface can be defined in the form of a physical grid for guiding intensity probe over the scanned surface. For the rectangular duct used in the present study a test surface of dimensions 0.48m x 0.56m x 1.28m is created surrounding the duct walls.

Thus there will be four surfaces one each surrounding the four walls of the duct.

The dimensions of top and bottom surface are 0.42 m x1.28 m and dimensions of the side surfaces are 0.56 m x1.28 m. Each surface is then divided into 2 rows and 4 columns to create small segments.
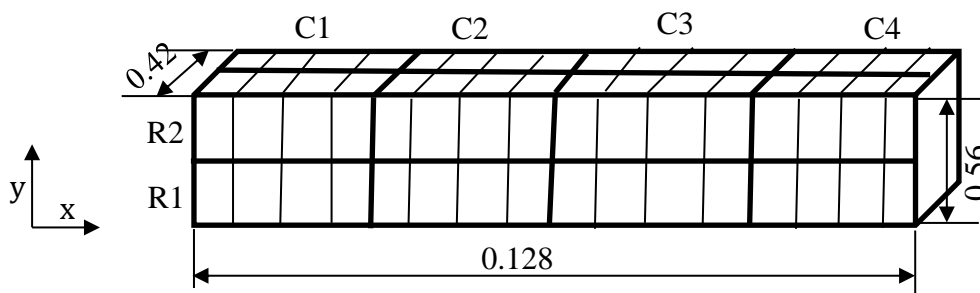
Figure 3.19: Schematic of the grid for the top and side surface of the duct

This kind of set up is done in the B & K hand held analyzer using the sound intensity template and set up preference. Figure 3.19 shows the schematic of the grid for the top and side surface of the duct

R1 and R2 indicate the row index and C1, C2 C3 and C4 indicate the column index.

3.3.3.2 Measurement procedure

Sound intensity measuring probe is scanned slowly over each segment by taking two perpendicular scans. Special care should be taken such that the measuring probe is always normal to the surface during scanning over virtual surface. Each segment records the sound intensity values. The data is then post processed using BZ-7233 sound analyzer software to extract sound power, sound pressure and sound intensity values for the measured surface. Figure 3.20 shows the sound intensity probe scanning the scanned surface

Figure 3.20: Sound intensity probe oreintation over the scanning the virtual surface.

Chapter 4

Results and Discussion

Validation of analytical, numerical and experimental results has been discussed in this chapter. Validation results for free vibration analysis, forced vibration response and sound power radiation has been reported between three methods.

4.1   Validation of Theoretical model

Duct dimensions mentioned in chapter 2 in section 2.1 is used for validation studies.

Uncoupled structural analysis

The first ten uncoupled structural natural frequencies of the rectangular duct for a given dimension as mentioned in section 2.1 subjected to simply supported boundary conditions using analytical and numerical methods are shown in Table 4.1.

It is observed that analytical and numerical results are in a very good agreement and with empirical results .Empirical equations given in reference[19]are used to find the first four modes of the rectangular duct.Equivalent plate model is appropriate to explain the free vibration behavior of a rectangular duct for further studies.

Table 4.1: First ten uncoupled structural modes of rectangular duct subjected to simply supported boundary condition

Mode	Analytical (Hz)	Numerical (Hz)	Empirical (Hz)
1	99.26	99.22	100.21
2	114.65	114.59	117.92
3	130.95	127.08	133.04
4	140.59	140.51	146.65
5	142.72	141.94	-
6	163.98	163.47	-
7	177.29	177.17	-
8	195.67	189.68	-
9	196.05	195.60	-

10	209.76	208.72	-

Figure 4.1a and Figure 4.1b show the structural mode shape for the fundamental duct mode at 99.26 Hz for an unfolded equivalent plate representation and numerical model. Figure 4.2a and Figure 4.2b shows the mode shape for mode 10 at 209.76 Hz for an unfolded equivalent plate representation and numerical model.
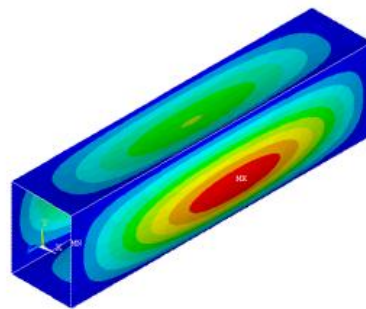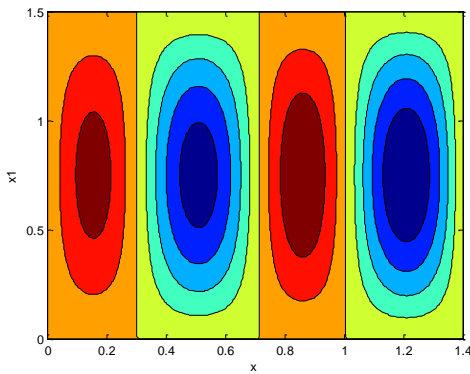
Figure 4.1a: Fundamental structural duct Mode shape at 99.26 Hz-Analytical

Figure 4.1a: Fundamental structural duct mode shape at 99.26Hz-Numerical
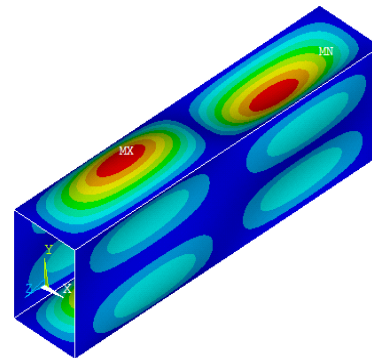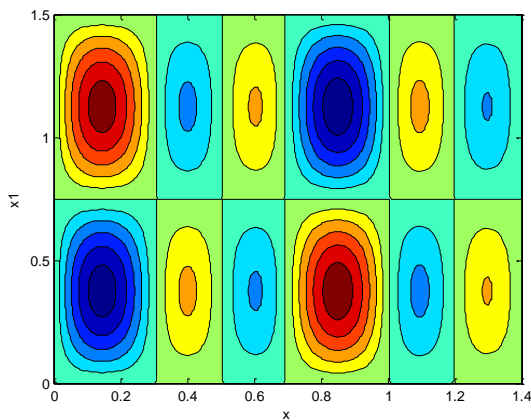
Figure 4.2b: Tenth duct mode shape at 209.76 Hz 209.76 Hz -Analytical

Figure 4.2b: Tenth duct mode shape at 209.76 Hz –Numerical

41

Structural modal analysis helps in understanding the displacement pattern of the structure subjected to a given boundary condition. The displacement pattern is expressed in terms of mode shape. Every mode shape is described in terms of modal indices which are described by the number of antinodes on a given panel in coordinate directions. Details of mode notation are described in section 4.1.2

In Figure 4.1a and Figure 4.2a the number of antinodes for the unfolded plate with x-x_1 coordinate system is shown. Along x from 0 - 0.3 is the +y panel pair from 0.3 - 0.7 is the +x panel pair from 0.7-1 is the $-x$ panel pair and from 1-1.4 is the $-y$ panel pair. The total length along x is equal to the perimeter of the plate which is equivalent to duct cross section in the numerical model.

Figure 4.1a shows that the number of antinodes on all duct plate panels is one .The same is observed in Figure 4.1b in the numerical model calculated using FEM approach.

Figure 4.2a shows the number of antinodes on y panel pairs is two along x_1 and one along x and the number of antinodes on x panel pairs is two along x and two along x_1.Similar kind of behavior is observed in the numerical model shown in Figure 4.2b

It is concluded from above results that the mode shape of equivalent plate model and FEM mode shape are representating the same behavior

Mode shape representation ,grouping and calculating net volume displacement

The structural mode shapes are analyzed to understand the free vibrational behavior of rectangular duct based on the modal grouping. This grouping helps to understand the symmetry behavior between the panel pairs and the relative change of phase between the panel pairs.

A particular notation based on natural frequency, number of anti-nodes on panel pairs and symmetry behavior is used to describe the each individual mode shape for categorizing different groups.It will be useful to form different groups. The fundamental structural mode shape shown in Figure 4.3a-e can be represented as [D_S (1, 1), S (1, 1)] $_{99.2\,Hz}$ according to the new notation. This can be described

with reference to Figures 4.3a - 4.3d as follows: the first term in the bracket indicates the number of antinodes at x panel pairs along y and z directions and that panel pair dominates in the amplitudes of the displacements and the second term indicates the number of antinodes on y panel pairs along x and z directions. Letter S or AS denotes symmetry or anti-symmetry mode shape behavior of duct walls.
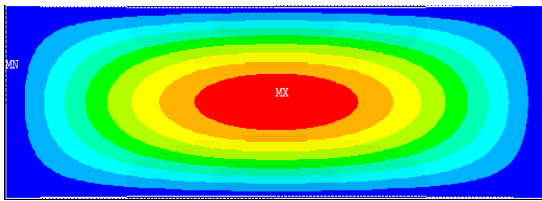
Figure 4.3a : Contour plot at x = 0.15
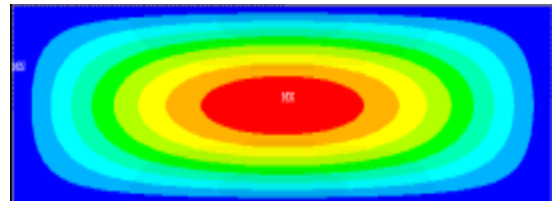
Figure 4.3b : Contour plot at x = -0.15
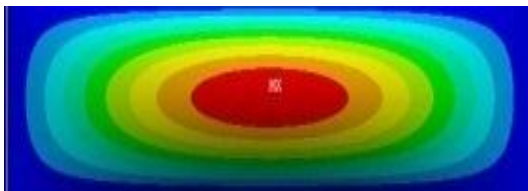
Figure 4.3c : Contour plot at y = 0.2
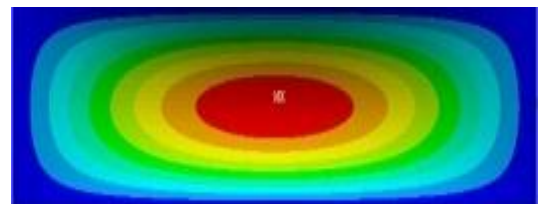
Figure 4.3d : Contour plot at y = -0.2
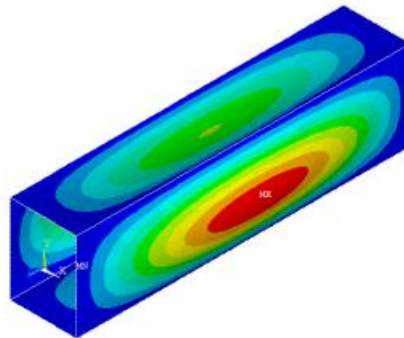
Figure 4.3e: Isometric view of Fundamental mode shape of duct ([D_S (1, 1), S (1, 1)]) $_{99.2Hz}$

Table 4.2 gives the grouping of first thirty modes with simply supported boundary conditions and also the corresponding net volume displacements.

There are four groups based on mode symmetry and anti-symmetry behavior. Group1 represents Symmetry (S)-Symmetry (S) behavior of x-axis pair and y-axis pairs. Similarly, the other three groups are S-AS, AS-S and AS-AS.

Table 4.2: Various Groups of duct modes and net volume displacements for each mode

	Mode No		Net volume displacement
group 1	1	$[D\_S(1,1),S(1,1)]_{99.2\ Hz}$	0.1182
	2	$[D\_S(1,2),S(1,2)]_{114.59\ Hz}$	0
	4	$[D\_S(1,3),S(1,3)]_{140.5Hz}$	0.0421
	7	$[D\_S(1,4),S(1,4)]_{177.17Hz}$	0
	11	$[D\_S(1,5),S(1,5)]_{224.69Hz}$	0.0277
	14	$[S(1,1)^*,D\_S(1,1)]_{248.96Hz}$	0.2630
	16	$[S(1,2)^*,D\_S(1,2)]_{259.43Hz}$	0
	18	$[S(1,3)^*,D\_S(1,3)]_{278.08Hz}$	0.0868
	19	$[D\_S(1,6),S(1,6)]_{283.08Hz}$	0
	21	$[S(1,4)^*,D\_S(1,4)]_{306.25Hz}$	0
	23	$[S(1,5)^*,D\_S(1,5)]_{345.11Hz}$	0.0512
	24	$[D\_S(1,7),S(1,7)]_{352.37Hz}$	0.0216
	29	$[S(1,6)^*,D\_S(1,6)]_{395.46Hz}$	0
group 2	3	$[D\_AS(1,1),S(2,1)]_{127.08Hz}$	0
	5	$[D\_AS(1,2),S(2,2)]_{141.94Hz}$	0
	6	$[D\_AS(1,3),S(2,3)]_{163.47Hz}$	0
	9	$[D\_AS(1,4),S(2,4)]_{195.60Hz}$	0
	13	$[D\_AS(1,5),S(2,5)]_{239.22Hz}$	0
	20	$[D\_AS(1,6),S(2,6)]_{294.53Hz}$	0
	25	$[D\_S(1,7),S(2,7)]_{361.47Hz}$	0
group 3	8	$[S(2,1),D\_AS(1,1)]_{189.68Hz}$	0
	10	$[S(2,2),D\_AS(1,2)]_{208.72Hz}$	0
	12	$[S(2,3),D\_AS(1,3)]_{233.06Hz}$	0
	17	$[S(2,4),D\_AS(1,4)]_{267.39Hz}$	0
	22	$[S(2,5),D\_AS(1,5)]_{312.34Hz}$	0
	26	$[S(2,6),D\_AS(1,6)]_{368.20Hz}$	0
group 4	27	$[D\_AS(2,2),AS(2,2)]_{375.41\ Hz}$	0
	30	$[D\_AS(2,3),AS(2,3)]_{403.43Hz}$	0

Net volume displacement for each uncoupled structural mode is calculated numerically based on Equation 2.25 to understand which mode is efficiently radiating sound and for characterizing the kind of sound sources. It is observed from

Table 4.2 that all (odd, odd) modes have relatively large net volume displacement in group 1(S-S) than remaining all the modes that have zero values. The mode that has the symmetrical panel pairs and the largest net volume displacement in group 1 can be identified to be an efficient sound radiator with a monopole kind of sound source. Modes having (odd, even) or (even, odd) mode shapes in group 1 behave as dipole and are less efficient sound radiators. It can be observed by calculating radiation efficiency and also their slope.

Calculation of modal radiation efficiency for plate

Radiation efficiency for simply supported plate has been validated using literature results numerically [27]. Structural natural frequencies corresponding to various modes and corresponding modal indices are mentioned in reference [27]

Dimensions of the plate are length $a = 0.414$m Width $b = 0.314$m and thickness h=2mm

Aluminum material properties are applied to the plate

Figure 4.4 shows the radiation efficiency curve for the first six modes of the simply supported rectangular plate [27].
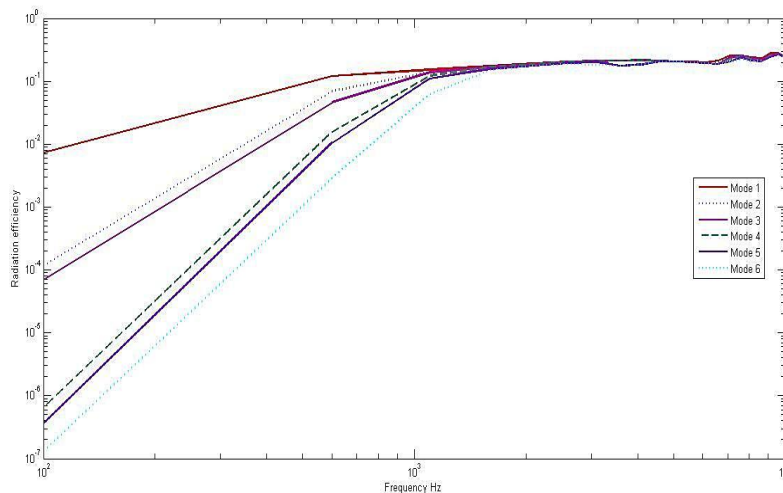
Figure 4.4: Radiation Efficiency of first six modes of simply supported rectangular plate

It is observed from Figure 4.4 that the radiation efficacy for the mode 1 is highest compared this all other modes. This mode correspond to the (1, 1) mode of the plate. From here it can be said that (odd, odd) fundamental mode is the most efficient sound radiatior.The radiation efficiency curves exhibit a slope behavior till the cut

off frequency. Radiation efficiency curves become asymptotic after the cut off frequency. Cut off frequency for simply supported plate calculated using the Equation 2.37 is at 5866 Hz and it is observed from that graph that the curves become asymptotic after this frequency.Similar behavior is observed for all the modes.

Calculation of modal radiation efficiency for one structural mode coupled to multiple acoustic modes

Figure 4.5a shows the modal radiation efficiencies corresponding to modes in group [D_S, S] .A good agreement with the analytical and numerical results can be found. All the modes in this group with (odd, odd) modal indices exhibit the same behavior as that of a simply supported panel (1.4 m x 1.5 m) with (1, 1) mode.
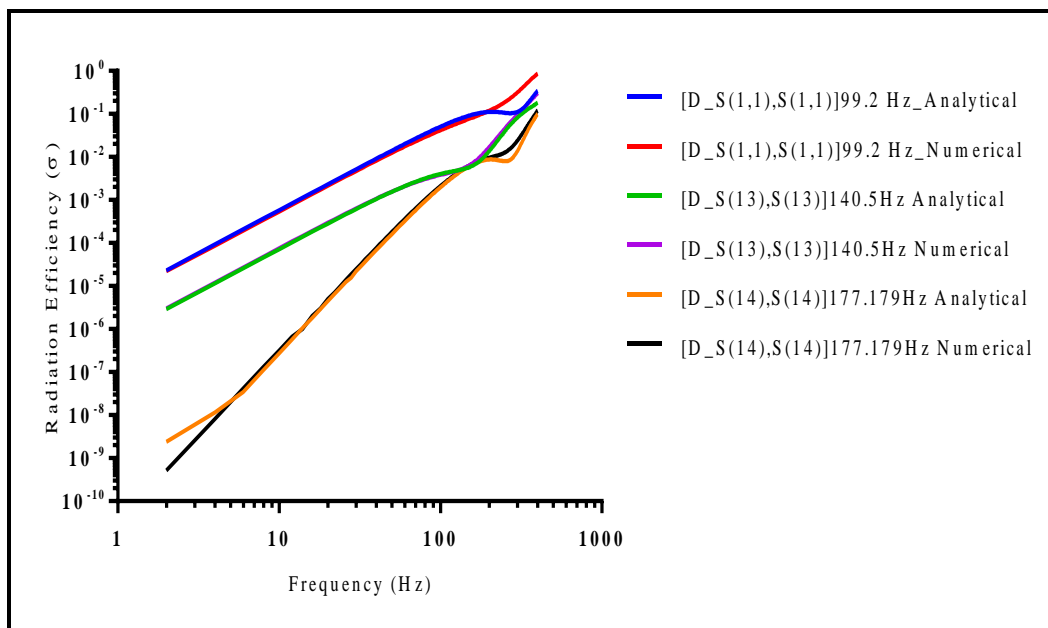
Figure 4.5a Comparison of analytical and numerical models of duct modal radiation efficiency for [(D_S, S)] group

Figure 4.5b shows the comparison of (1, 1) plate mode of simply supported panel with the [D_S, S] group. All the modes in the group1 with (odd, odd) modal indices exhibit the same slope of 20 dB/decade as that of the simply supported panel (1.4 m x 1.5 m) till the cut off frequency of 166.16 Hz calculated using Equation 2.37.

46
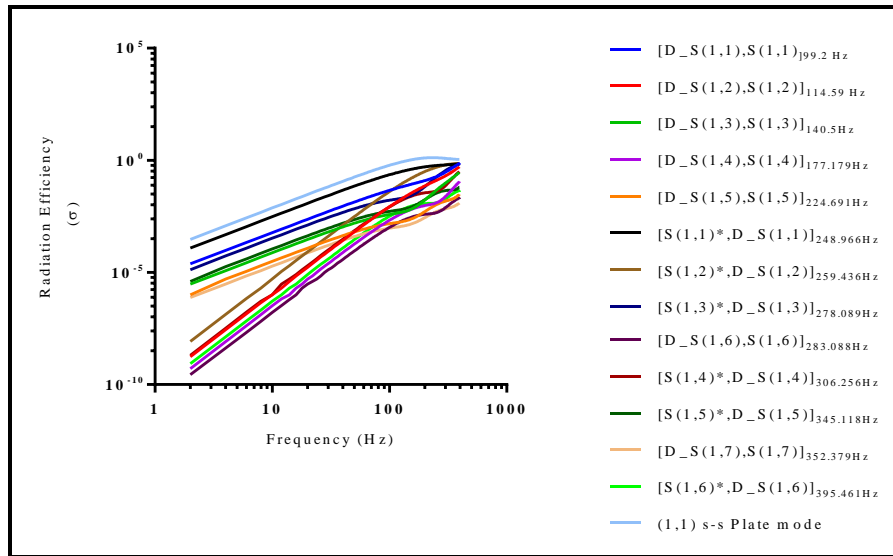
Figure 4.5b: Calculation of duct modal radiation efficiency with respect to frequency for [(D_S, S)] group

After this the curve becomes asymptotic and the radiation efficiency curve approaches to unity. Details of the slope values for few of the selected modes for various groups are shown in Table 4.3.

Figure 4.6a and shows the variation of modal radiation efficiencies corresponding to [D_AS, S] group. It is observed that analytical and numerical results are in good agreement. Slope is higher compared to group 1. It is consistent with observation made based on volume displacement. Figure 4.6b shows the comparison of modal radiation efficiencies with that of a simply supported panel of (2, 1) mode. Simple supported plate with equivalent dimensions has same slope as a duct with group2 mode shape but it has higher slope values compared to lower mode in the duct mode group 2. The slope behavior of 40 dB/decade is observed till the cut off frequency of 268 Hz after that the values approach to unity and the curve becomes asymptotic. Radiation efficiency values are lower for higher modes compared to fundamental mode. As mentioned this kind of slope behavior is observed till cut off frequency
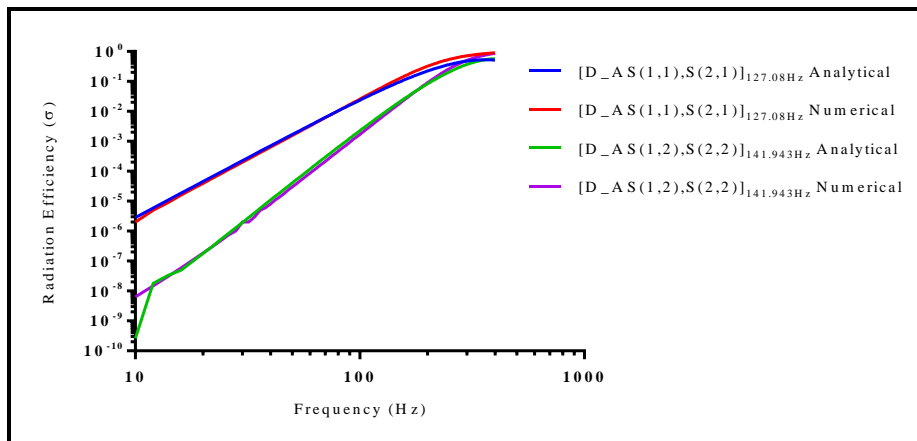
Figure 4.6a: Comparison of analytical and numerical model results for a duct Modal Radiation efficiency for [D_AS, S] group
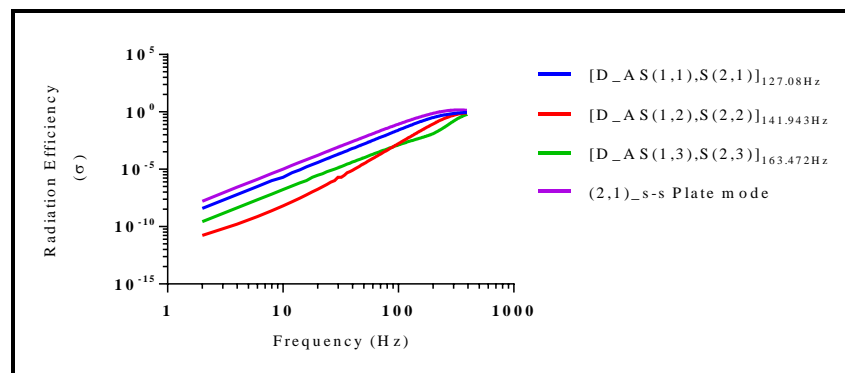
Figure 4.6b: Calculation of duct modal radiation efficiency with respect to frequency for [D_AS, S] group

Figure 4.7a shows the variation of modal radiation efficiencies corresponding to [S, D_AS]; Slope value of this group of modes is same as [D_AS, S] group. Analytical and numerical results are in good agreement. Figure 4.7b shows the comparison of modal radiation efficiencies with that of a simply supported panel with (1, 2) mode shape.Behaviour of radiation efficiency curves for [S, D_AS] and [D_AS, S] is similar and they exhibit a slope behavior as that of a (1, 2) simply supported panel with a value of 40dB/decade till the cut off frequency of 257.1Hz.

48
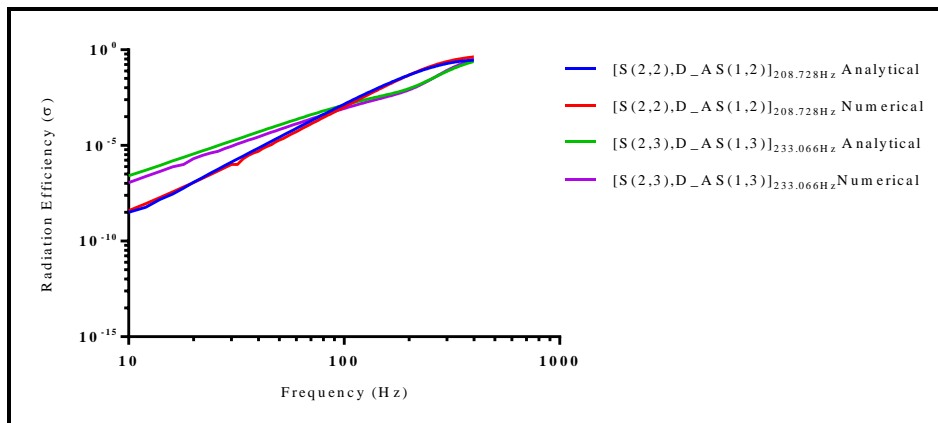
Figure 4.7a: Analytical and Numerical comparison of Modal Radiation efficiency for [S, D_AS] group
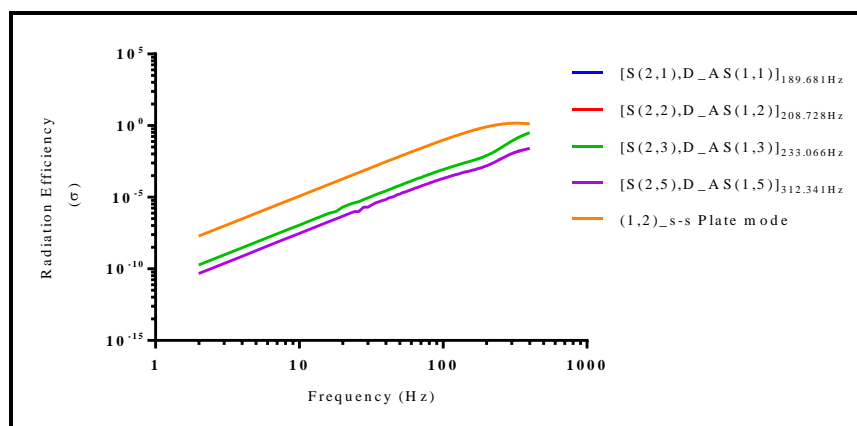
Figure 4.7b: Calculation of duct modal radiation efficiency with respect to frequency for [S, D_AS] group

Figure 4.8a shows the comparison of numerical and analytical modal radiation efficiencies corresponding to [D_AS, AS]. Figure 4.8b shows the comparison of modal radiation efficiency with simply supported panel for [D_AS, AS] group. All the modes in this group have (even, even) modal indices and exhibit similar slope as that of the simply supported panel (1.4 m x 1.5 m) of 60 dB/decade with (even, even) modal indices. The slopes of these curves are the highest compared to any other group.The cut off frequency for the plate mode occurs at 332.2 Hz.After the cut off the radiation efficiency curve beomes asymptotic.
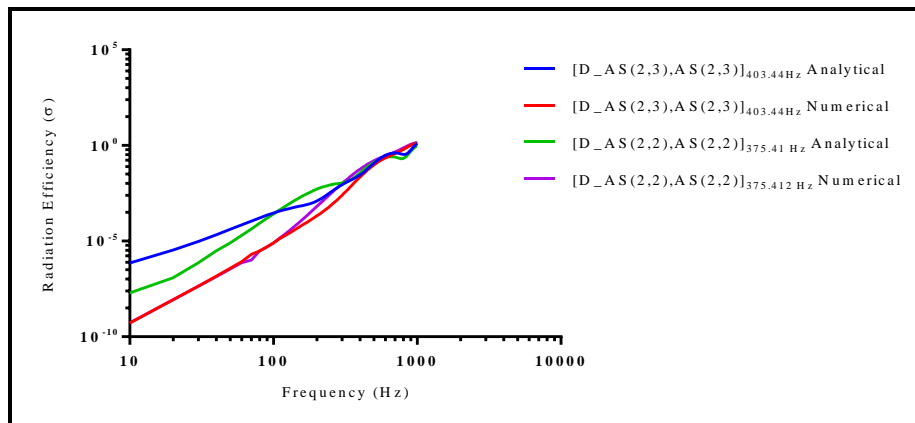
Figure 4.8a: Analytical and numerical comparison of Modal radiation efficiency for [(D_AS, D_AS)] group
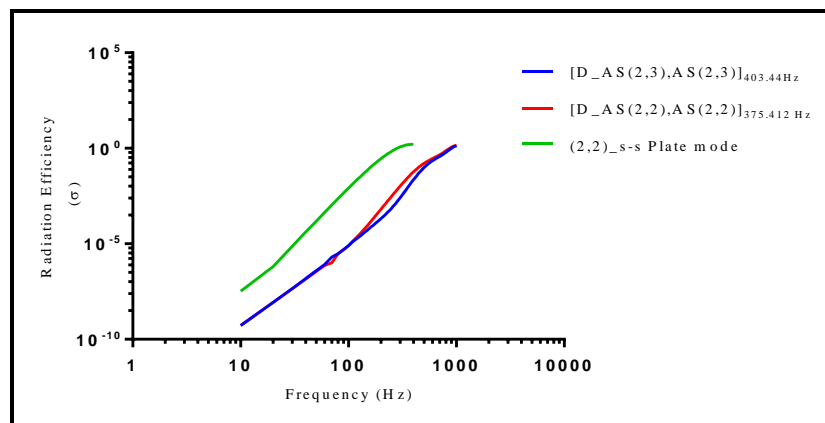
Figure 4.8b: Calculation of duct modal radiation efficiency with respect to frequency for ([D_AS, AS])

Table 4.3 shows a comparison of slope for selected modes from all the four groups for duct modes and simply supported plate modes. It is observed that duct radiation efficiency slope values of all groups are same as equivalent plate radiation efficiency slope rates. It can be concluded that duct radiation efficiencies of different groups can be calculated based on equivalent plate model with minimum error. Equivalent plate model for a rectangular duct proposed in this research work is an ideal to predict free vibration behavior and sound radiation characteristic of a duct.

Table 4.3: Comparison of the radiation efficiency slopes for duct modes and simply supported plate modes

Group	Duct Mode	Duct mode –Analytical (dB/decade)	Duct mode –Numerical (dB/decade)	Simply supported Plate mode (dB/decade)
1	[D_S(1,1),S(1,1)]99.2 Hz	19	19	19
2	[D_AS(1,1),S(2,1)]127.08Hz	41	41	39
3	[S(2,3),D_AS(1,3)]233.06Hz	37	39	39
4	[D_AS(2,2),AS(2,2)]375.41Hz	57	58	54

Calculation of radiation efficiency for an uncoupled flexible duct

Figure 4.9 shows a comparison of radiation efficiency of a rectangular duct for uncoupled condition (no acoustic volume) and coupled with acoustic volume (i.e., one structural mode coupled to multiple acoustic modes). It can be observed from the graph that both the conditions show a similar kind of behavior. Coupling of single structural mode with multiple acoustic modes behavior is same as that in uncoupled behavior. Duct sound radiation behavior is becoming independent of type of excitation.
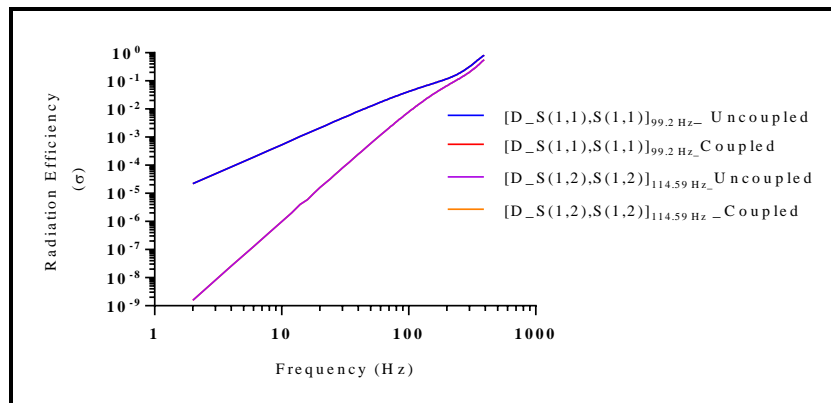
Figure 4.9: Comparison of coupled and uncoupled radiation efficiencies

Calculation of radiation efficiency for strongly coupled structural modes.

Figure 4.10 shows the radiation efficiencies for the one structural mode coupled to multiple acoustic modes.Coupled structural mode is identified based on the transfer factor value. Transfer factor defined in Equation 2.33 is used to identify structural modes which have the high transfer factor values as a prone to strong coupling with acoustic mode. The structural mode frequencies with highest transfer factor are identified and then coupled to multiple acoustic modes to calculate the radiation efficiency.

It is observed from the graph that mode 14 (249.85 Hz) is the most efficient radiating mode followed by mode 1 (99.26 Hz).). It is observed from radiation efficiency values of individual groups that S-S (group1) with (odd-odd) indices is efficient sound radiator. The dominant panel for mode 14 has more flexible wall are compared to mode 1 dominant panel area. Controlling of vibration amplitude on dominant large panel area helps in reducing sound radiation.

It is also observed that net volume displacement of mode 14 is large compared to other modes. This is due to symmetry between the panel pairs of mode 14 at 249.85 Hz. Similarly, structural modes (1, 11, 14, and 18) at 99.2 Hz, 249.85 Hz, 224.69 Hz and 283.08 Hz. have the same kind of slopes which is a characteristic observed for (odd, odd) mode. A slope of 20dB/ decade is observed in (odd, odd) modes. Structural modes (2, 21) at 114.65 Hz and 306.25 Hz are (odd, even) modes which have a slope of 40 dB/decade.
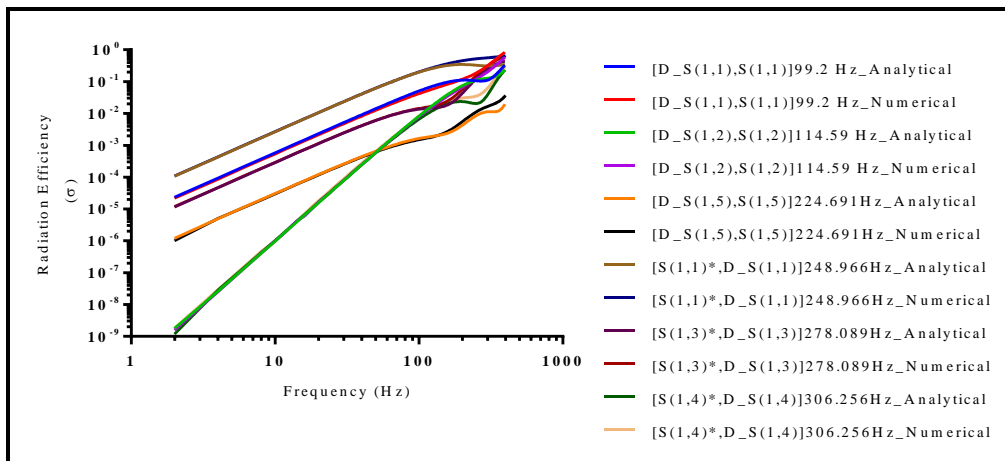
Figure 4.10: Variation of Modal radiation efficiency of strongly coupled structural modes

Table 4.4 shows the slopes of strongly coupled structural modes and also shows a comparison of slopes for analytical and numerical models. Radiation efficiency curves for single structural mode coupled to multiple acoustic modes and uncoupled mode behavior are found to be similar. So a comparison with the uncoupled plate radiation efficiency has been done for a single structural mode coupled to multiple acoustic modes.

Table 4.4: Radiation efficiency slopes of strongly coupled structural modes

Mode	Frequency(Hz)	Analytical (dB/decade)	Numerical (dB/decade)
1	99.26	19.42	18.90
2	114.65	39.25	39.00
11	224.84	17.27	16.96
14	249.85	18.72	18.74
18	278.08	16.75	16.90
21	306.25	38.05	38.69

Uncoupled Acoustic modes

Table 4.5 gives first ten uncoupled acoustic modes of the duct volume subjected to rigid termination boundary condition. The first Acoustic modes occur as per c/ (2 x length of largest dimension) criteria. In this case it is 340/ (2 x1.5) = 113.3 Hz

53

Table 4.5: First ten uncoupled acoustic modes of the duct volume with rigid termination

Mode No	Analytical (Hz)	Numerical (Hz)
1	113.3	113.3
2	226.7	226.6
3	340	340
4	425	425
5	439.9	439.8
6	453.3	453.3
7	481.7	481.6
8	544.3	544.2
9	566.7	566.6
10	566.7	566.6

Table 4.5 shows that the uncoupled acoustic modes estimated analytically and numerically are in a good agreement.

Coupled Vs. Uncoupled

Inside duct pressure and wall vibrations of a rectangular duct is calculated with analytical and numerical methods. Equations 2.23 and 2.24 are used in analytical model to calculate inside duct pressure and wall vibration velocity.

Variation of the inside duct pressure at a point $(0.5 \times L_2, 0.5 \times L_3, 0.4 \times L_1)$ with respect to frequency is shown in Figure 4.11a and Figure 4.11b. Figure 4.11a shows sound pressure inside the duct for a coupled and uncoupled condition. Figure 4.11 b shows the result comparison between numerical and analytical modes for a couple system.

It is observed from the graph that the first peak in uncoupled model curve occurs at 113 Hz which corresponds to the uncoupled acoustic mode and it is observed that in the same region in coupled curve that the energy due to uncoupled acoustic mode is split into two coupled frequencies at 104 Hz and 122 Hz which correspond to the first two peaks in coupled model curve.
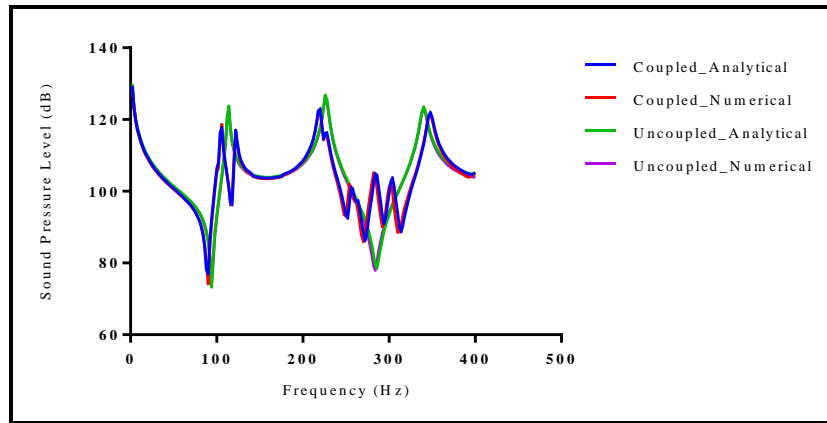
Figure 4.11a: Comparison of Uncoupled and coupled pressure inside the duct

From Figure 4.11b it is observed that the phenomenon of coupling occurs close to acoustic modes where an uncoupled frequency splits into two coupled frequencies which is a mode of energy due to acoustic modes. It is observed from the graph that a shift in natural frequency is noticed closer to the acoustic modes at113 Hz, 226 Hz and a dominant peak is noticed at 340 Hz.
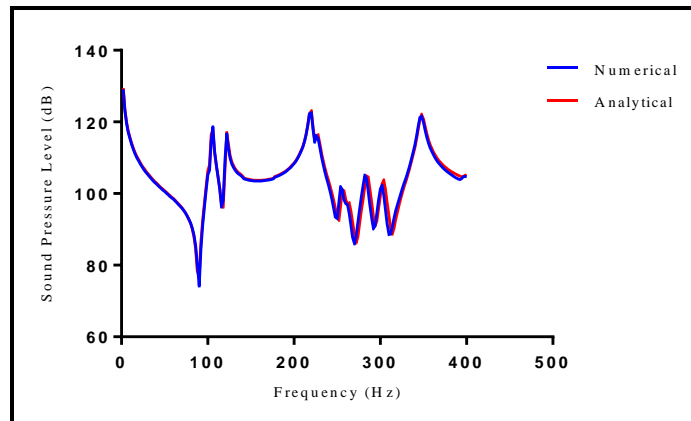
Figure 4.11b: Variation of inside duct pressure with respect to frequency

From Figures 4.11a and 4.11b it can be observed that the split in frequency at uncoupled acoustic frequency into two frequencies explains the coupling between acoustic and structural modes. The energy exchange between acoustic and structural subsystems at coupling frequency converts as a multi-degree freedom system.

Table 4.6a gives the first thirty modes estimated numerically by coupled modal analysis. These coupled modes contain uncoupled acoustic modes,uncoupled

structural modes and coupled modes. It is observed from Table 4.6a that coupling occurs close to acoustic modes.

Table 4.6a: Coupled modes of a rectangular duct

Mode No	Frequency (Hz)	Mode No	Frequency (Hz)	Mode No	Frequency (Hz)
1	100.48	11	208.23	21	282.82
2	105.36	12	219.39	22	294.39
3	121.47	13	226.30	23	301.62
4	126.61	14	232.59	24	311.92
5	140.08	15	238.81	25	343.82
6	141.47	16	254.16	26	347.07
7	162.99	17	258.02	27	352.22
8	177.12	18	260.92	28	361.28
9	189.14	19	266.91	29	367.71
10	195.22	20	282.74	30	374.89

Table 4.6b: Comparison of Uncoupled and Coupled modes

Uncoupled Mode Frequency (Hz)	Mode type	Coupled mode Frequency(Hz)
99.22	structural	100.48
113.3	acoustic	105.36
114.59	structural	121.47
127.08	structural	126.61
140.51	structural	140.08
141.94	structural	141.47
163.47	structural	162.99
177.17	structural	177.12
189.68	structural	189.14
195.60	structural	195.22
208.72	structural	208.23
224.69	structural	219.39

226.6	acoustic	226.30
345.1	structural	343.82
345	acoustic	347.07

It is seen from Table 4.6b that acoustic mode at 113.3 Hz and structural mode 114.59 are strongly coupled .This is observed by a shift in a natural frequency due to coupled modes at 105.36 Hz and 121.47 Hz. The structural mode at 345.1Hz and acoustic mode at 345 Hz have strong coupling which can be noticed due to shift in the natural frequency due to coupled modes at 343.82 Hz and 347.07 Hz

Calculation of modal radiation efficiency for one acoustic mode Coupled to multiple acoustic modes

In order to understand the effect of coupling closer to acoustic mode, one acoustic mode is coupled to multiple structural modes are considered. Figure 4.10 shows the radiation efficiency corresponding to the strongly coupled acoustic modes. Mode 1 of acoustic at 113.3 Hz is closer to the structural mode 2 (114 Hz) and second acoustic mode is strongly coupled to structural modes 11, 14, 17 (224 Hz, 248.96 Hz, 279.36 Hz). Third acoustic mode is strongly coupled to structural mode 20 (307.82 Hz).

Table 4.7 shows the transfer factor values for strongly coupled acoustic modes. It is observed from the Table 4.7 that a strong coupling exists between the acoustic mode at 113.3 Hz and Structural mode at 114.7 Hz. Transfer factor values close to 1 represents a strong coupling. Generally, closer uncoupled acoustic and structural natural frequencies and good spatial matching of mode shapes provides higher transfer factor values.

Table 4.7: Transfer factor values for strongly coupled acoustic modes

Acoustic Mode (Hz)	Structural Mode (Hz)	Transfer Factor $T_{n,m}$
113.3	114.7	1.37

	224.9	0.18
226.6	248.96	0.12
	278.08	0.17
340	306.06	0.14

Figure 4.12 shows the radiation efficiency of first three acoustic modes individually coupled to all structural modes with respect to frequency.
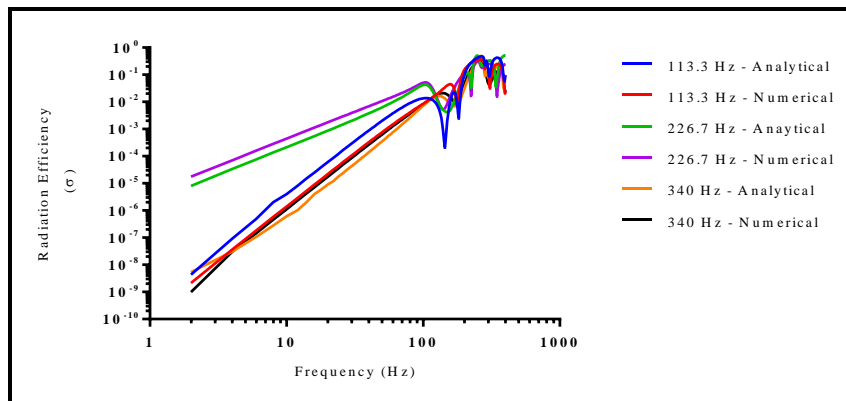
Figure 4:12: Radiation efficiency of the first three acoustic modes

It is observed that second acoustic mode is more efficiently radiating sound since it is strongly coupled to three structural modes compared to the other two acoustic modes.
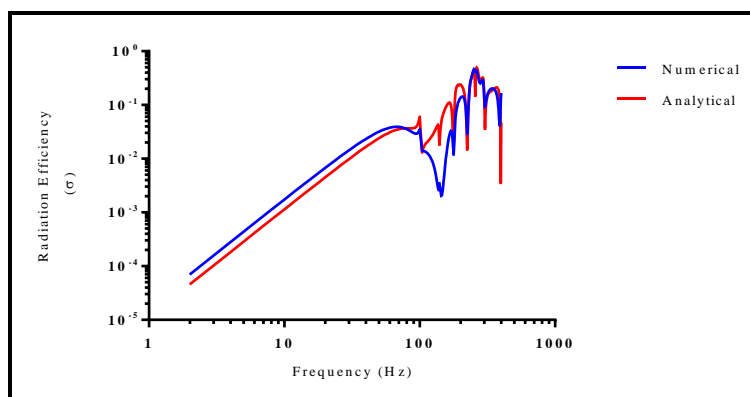
Figure 4.13: Total radiation efficiency of rectangular duct

Figure 4.13 and Figure 4.14 shows the total radiation efficiency and the total sound power radiated with multiple acoustic modes coupled to multiple structural modes. All the peaks in the sound power curve correspond to the coupled modes. The first peak in the total sound power curve occurs at the coupled modes 106 Hz and 122Hz where the acoustic energy is split due to the acoustic mode at 113.3 Hz. The next prominent peaks in the curve occur close to second acoustic mode at 226.6 Hz where acoustic energy is exchanged among three structural modes. The next prominent peaks occur close to third acoustic mode at 340 Hz.
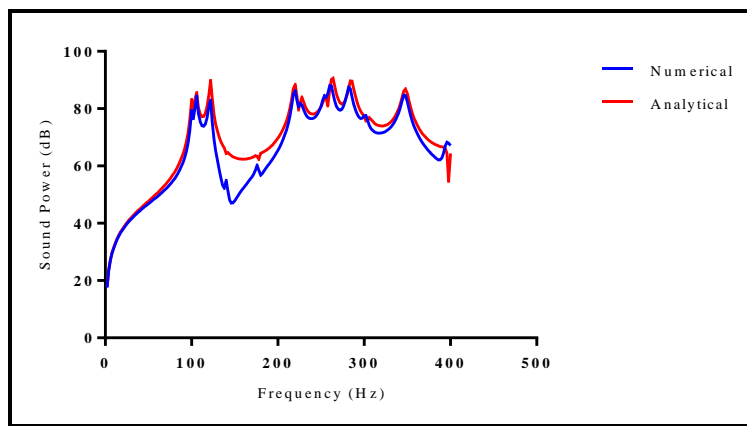
Figure 4.14: Total sound power radiated from the rectangular duct

Figure 4.15a represents pressure distribution at a point on x panel (x=0.2m, y=-0.068m, z=-0.609m) and y panel(x=-0.066m, y=0.25m, z=-0.609m) respectively. All the peaks correspond to coupled frequencies (from Table 4.6a) can be observed. Figure 4.15b represents the sound pressure distribution at different frequencies on the field point mesh (radiation mode shape) of acoustic mode at 340Hz coupled to structural modes these radiation mode shapes are calculated with numerical models.This mode shape is close to structural mode shape (306 Hz) which has dipole behavior where strong coupling is observed.It can be observed that sound radiation behavior strongly dependent on structural vibration distribution.
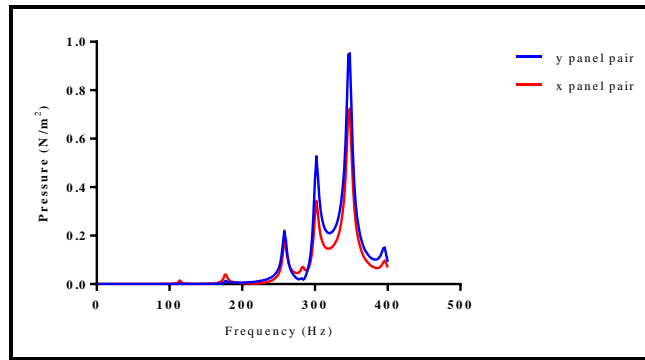
Figure 4.15a: Calculation of pressure at field point at x panel pair (0.2m, -0.068m,-0. 609m) and y panel pair (-0.066m, 0.250m, -0.609m)
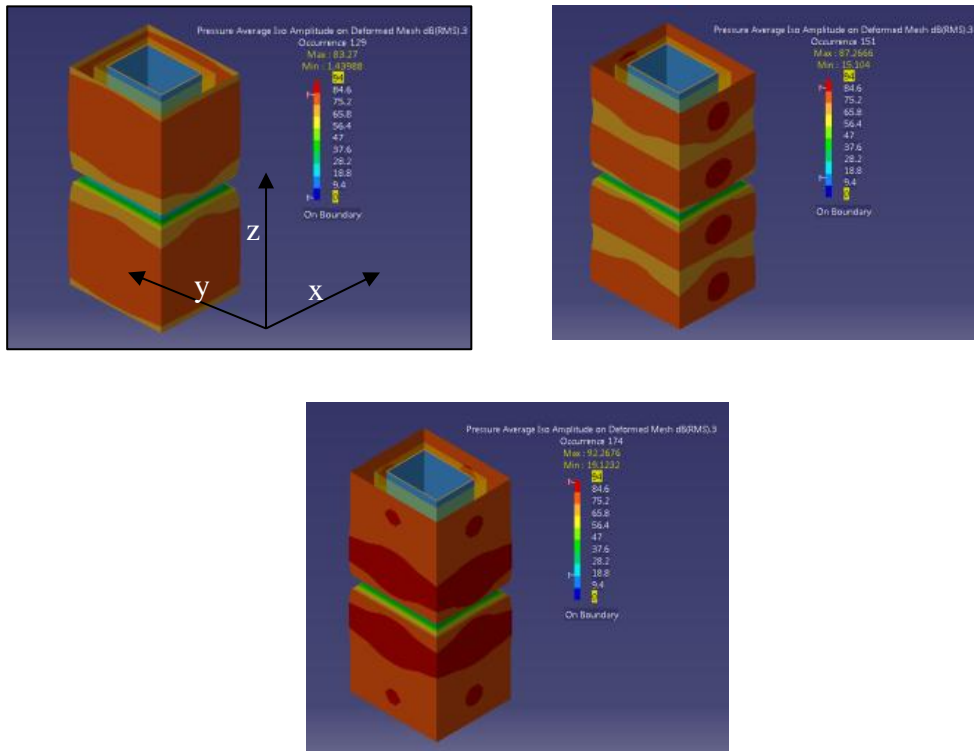
Figure 4.15b : Numerical Calculation of radiation mode shape for acoustic mode at 340 Hz

It can be summarized based on the above results that analytical and numerical results are in good agreement to capture acoustic & structural behavior of coupled and uncoupled sub-systems. Proposed equivalent plate model for a rectangular duct is able to explain the free vibration behavior and sound radiation characteristics. Modal grouping based on free-vibrational study shows that group1 (Symmetry-

Symmetry) modes with (odd-odd) indices are more efficient sound radiator. It is justified based on radiation efficiency results.

4.2   Validation of Experimental model

This section describes the validation results of experimental setup and also shows the comparison of different results with analytical and numerical model results.

The rectangular duct dimensions of L1 =1.2 m, L_2=0.3m, L_3=0.4 m have considered for experimental study and the coordinates of the duct are shown in Figure 2.5a. Material properties of the duct are Galvanized steel (GI) with Young's modulus E =200 Gpa, poisons ratio υ =0.29, and density ρ_s=7850 kg/m^3

Acoustic excitation in the form of pink noise is given to the duct by means of speaker mounted on the front plate of the duct. The same input is to be given in the numerical model where the particle velocity in the form of velocity boundary condition should be given. Particle velocity of 0.001 m/sec is given as input in theoretical model. This is obtained by measuring sound pressure level at far field of the speaker surface which is at a distance of 10 cm from speaker surface. Dimensions of field point mesh considered are 0.42 m x 0.56m x 1.2m (x=0.42m, y=0.56m, z=1.2m) (reference Figure 2.8 for coordinate directions)

Figure 4.16 shows the variation of wall displacement at location x=0.15, y=0.2, z=0.57(reference Figure 2.7a for coordinate directions). It shows the comparison of results from analytical, numerical and experimental models. There are two uncoupled acoustic mode till 400 Hz and the first acoustic mode occurs at 141.6 Hz and the second one occurs at 282 Hz (from numerical acoustic modal analysis).
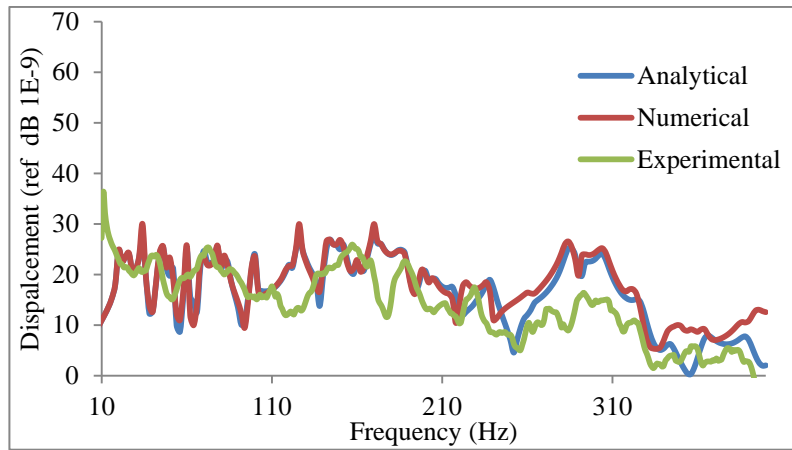
Figure 4.16: Duct wall displacement at x=0.15, y=0.2, z=0.57

It is observed from the graph that near the region of first acoustic mode (141.46 Hz) prominent peaks are observed and the next dominant peaks are noticed near the region of second acoustic mode at 283 Hz. This shows that the phenomenon of coupling occurs close to acoustic modes.Figure 4.17 shows the normalized wall displacement along the mid cross section plane of the duct measured at 142 Hz which is closer to first acoustic mode. Experimental results and numerical results are in agreement in predicting normalized wall displacement behavior but there is a discrepancy in amplitude. It is observed that there is difference in experimental and numerical in plate 1 due to the joint in the experimental duct. Joint along the length creates lot of discrepancy with analytical and numerical results based on ideal shape of rectangular duct. Assumption of ideal rectangular duct shapes in theoretical model is not able to capture variation in stiffness due to the joint. Further studies are required to understand the effect of joint on vibrational behavior.
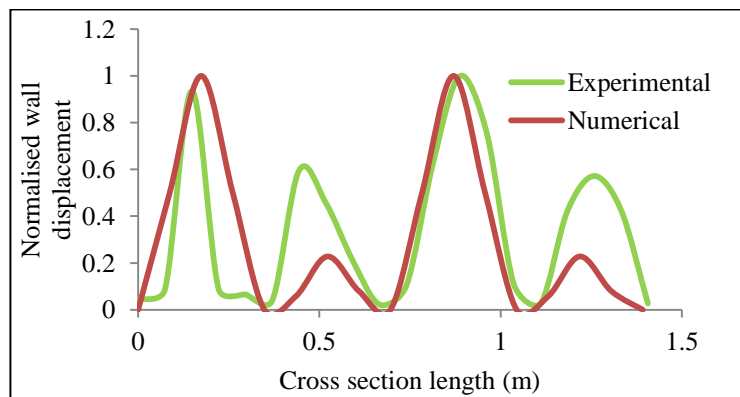
Figure 4.17: Normalized Wall displacement along the cross section measured at 142Hz
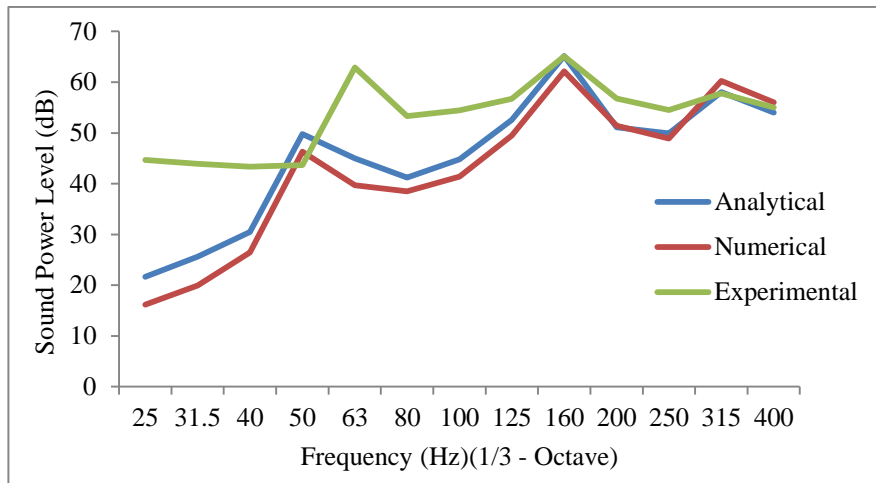
Figure 4.18: Total sound power radiated from the duct

Figure 4.18 shows the total sound power radiated from the duct. It is observed that experimental values are higher at low frequencies compared to numerical and analytical values. The first peak in experimental values occurs at 63 Hz center frequency which is due to uncoupled structural mode [(D_S(1,1),S(1,1))] at 65 Hz(from Experimental Modal analysis).The first peak in numerical and analytical models occurs at 50 Hz center frequency where the uncoupled structural mode [(D_S(1,1),S(1,1))] mode at 50 Hz exist (structural modal analysis).The second peak in all three models occur at 160 Hz center frequency where the first acoustic mode at 141.6 Hz exist. The third peak in all the three models occurs at 315 Hz center frequency where the second acoustic mode exists. It observed that experimental duct is stiffer compared duct considered in theoretical and numerical model.

Figure 4.19 shows the comparison of radiation efficiency graph for analytical, numerical and experimental data at 1/3 octave frequency. Experimental graph is not in good agreement with the numerical and analytical values till 125 Hz center frequency but the trend matches with analytical after from 160Hz.The values measures at low frequency deviates from the theoretical model which might be due to error in measuring sound power at low frequency and also due to high values in wall vibration velocity at low frequencies. The error can also be due to giving a constant velocity input source instead of a frequency dependent source (speaker characteristic)
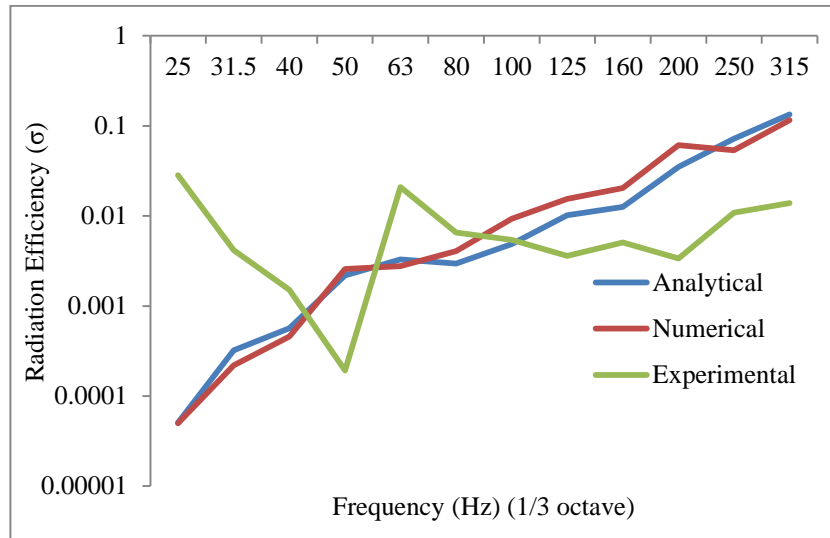
Figure 4.19: Comparison of radiation efficiency between three models

Figure 4.20a and 4.21b shows a comparison of sound pressure level measured at field point mesh x=0.42m, y=0.28m, z=0.3m (reference Figure 2.8 for coordinate directions) in dB scale and linear scale. It is observed from the graph that the overall trend in the variation of sound pressure level measured in experiment is matching with numerical data. Coupling phenomenon is observed due to presence of peaks in the region of acoustic modes at 141.6Hz and 283 Hz
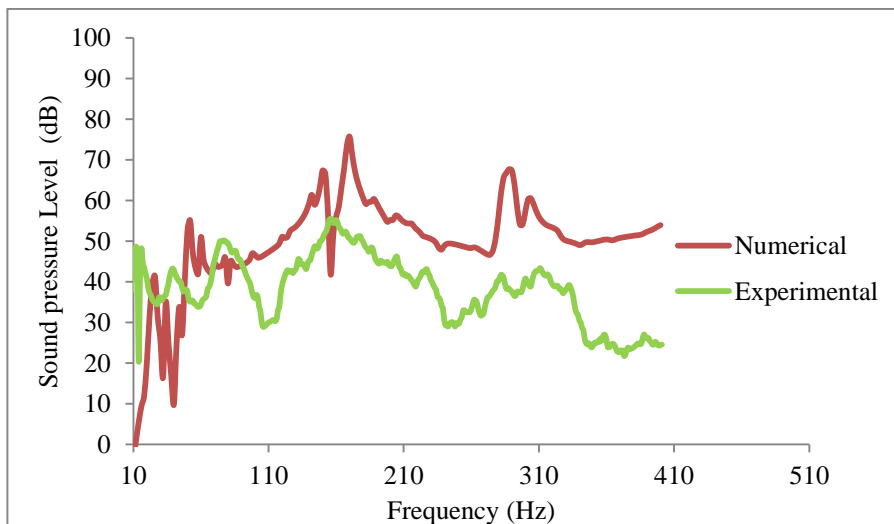
Figure 4.20a: Comparison of Sound pressure level on the field point mesh
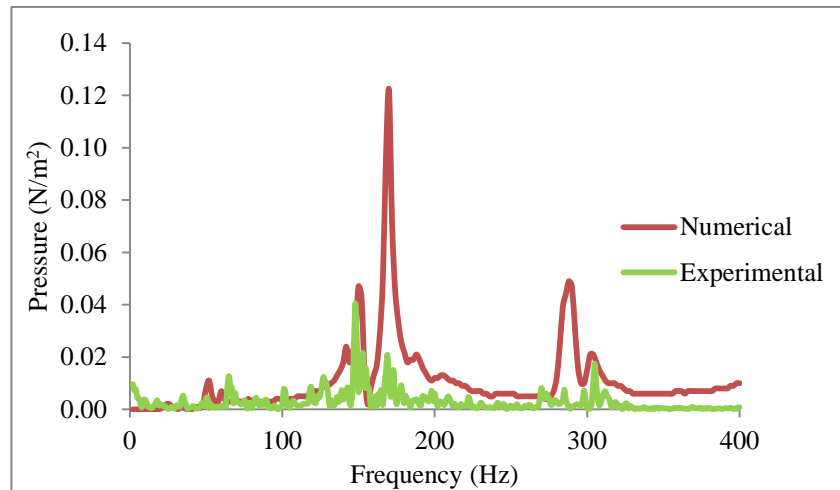
Figure 4.19b: Comparison of Sound pressure level on the field point mesh

Figure 4.21 shows a comparison of volume velocity for numerical and experimental models. It is observed from the graph that behavior in both the models matches but the amplitude in experimental values shows a lesser value at frequencies greater than 125 Hz center frequency. This is due to assumption of constant velocity input of the speaker where in actual sound pressure values of the speaker are fluctuating. Chosen experimental duct volume is representing acoustic volume in analytical and numerical models but structurally it is not. So, it shows a great discrepancy in amplitude and frequency below 100 Hz.
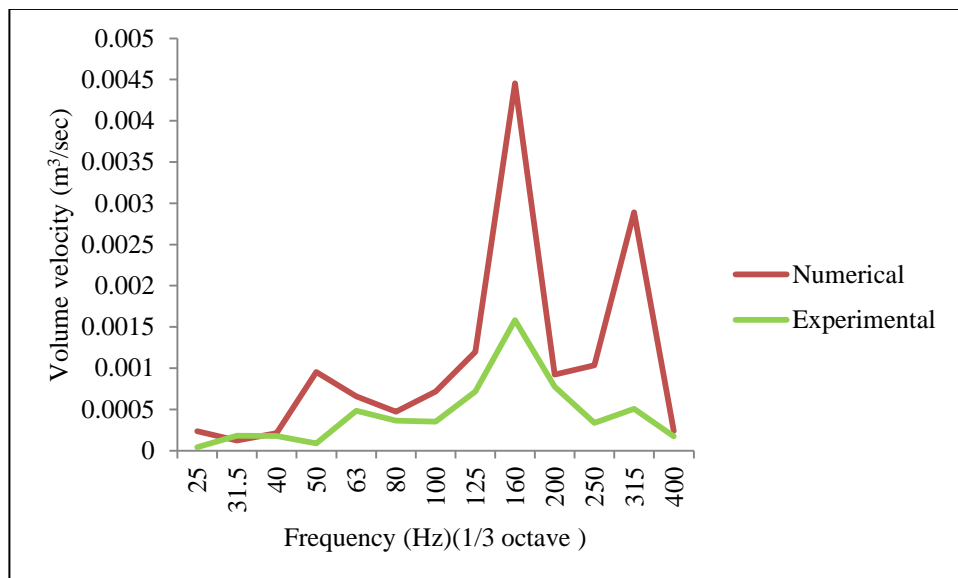
Figure 4.21: Comparison of numerical and experimental results of volume Velocity

The experimental data has to be further refined to reduce these deviations. A scope for improving the experimental set up is done by replacing the speaker with a constant source such as fan or any other speaker which has a sound pressure level values with +/- 3dB with respect to frequency. Modifying the experimental set up to reduce the noise coming in the front and back directions of the duct. The noise coming from back side of the speaker can be reduced by replacing the current enclosure made of plywood with that of a steel one which exhibits a good transmission loss at low frequencies.

The boundary condition of the duct has to be checked by doing a modal analysis of the duct for a free-free condition and correlate with the numerical model.

Chapter 5
Conclusion and Future work

Analytical, numerical and experimental studies have been conducted on a rectangular duct with simply supported structural boundary conditions and with a rigid end termination as acoustic boundary condition to determine various acoustic and structural parameters.

A validation of theoretical model has been done and a good agreement with the numerical results is found. Theoretical model is validated to estimate various acoustic and structural parameters. The uncoupled structural modes calculated using free vibration analysis is categorized into various groups and the net volume displacement is calculated for all the group of modes. It is found that Symmetry-Symmetry mode group with (odd, odd) modal indices behave as efficient sound radiators, which is determined from higher net volume displacement of (odd, odd) modes compared to other modes. Modal radiation efficiencies of one structural mode coupled to multiple acoustic modes is studied and the graphs are compared with the net volume displacement values of the structural modes to find out efficiently radiating mode due to acoustic excitation. Slopes of various group of modes have been studied and compared with simply supported panel to understand the behavior of duct in terms of plate modes. Modal radiation efficiencies are also calculated by coupling a single acoustic mode with multiple structural modes to understand the efficiently radiating acoustic mode. Duct radiation modes are correlated with that of standard sound sources such as monopole and dipole. A comparison study has been conducted for the inside duct pressures to understand the coupled and uncoupled behavior. It is observed that there is a shift in natural frequencies near to uncoupled acoustic modes due to coupling. The phenomenon of coupling exist always closer to acoustic modes. The total sound power radiated from the duct is estimated and also identified the dominant frequencies of sound power level which correspond to the coupled mode frequencies. These results help in identifying critical frequencies and controlling the sound power at critical frequencies.

An experimental set up has been developed for particular rectangular duct geometry to simulate the structural-acoustics phenomena of the rectangular duct. The complete experimental procedure is established to estimate various acoustic and structural parameters of the duct subjected to acoustic excitation. Vibration measurements have been done in order to calculate the wall displacement and wall vibration velocity. Sound intensity measurements have been conducted in order to determine the total sound power radiated from the duct. Wall displacement and pressure variation on the field point mesh around the rectangular duct have been measured to understand the effect of coupling at acoustic modes. Total radiation efficiency is estimated from the total sound power and wall vibration velocity measurements.

From the theoretical validation, it suggests that rectangular duct can be modeled as an equivalent plate for a free vibration analysis and sound radiation characteristics from duct walls. This helps in simplifying the radiation efficiency analysis of the duct from the known equations of the plate. The complete experimental methodology for estimating structural-acoustic parameters has been addressed and also the phenomenon of structural – acoustic coupling is identified in experimental study. All these results will be helpful to develop an active noise control methodology for the rectangular ducts.

Experimental results show some discrepancy in test results. So, the following modifications are suggested to the existing experimental setup. First one is to replace existing speaker with new speaker which supposed to provide a constant sound pressure level over an interested frequency range, especially lower frequency range. Another modification is about joint conditions in the rectangular duct. Based on the current results, it is observed that the experimental duct is behaving stiffer than the theoretical model. A further study required to understand joint properties on a duct wall and characterization these joints. Another suggestion is to improve the free vibration model to incorporate joint conditions in theoretical and numerical models. Other modifications required in experimental setup include a provision to measure sound pressure inside the duct and to control the break out noise by stiffening and by damping.

Appendix A

$$\Phi_m = \sum_{m_1}^{p_s} \sum_{m_2}^{q_s} A_{m_1,m_2} \sin\left(\frac{m_1 \pi x}{L}\right) \sin\left(\frac{m_2 \pi x_1}{L_1}\right)$$

$k_T k_\varphi$ are the linear and rotational spring stiffness

$$\sum_{m_1}^{p_s} \sum_{m_2}^{q_s} \left[C_{m_1 m_2 ij} - \lambda E_{m_1 i}^{00} F_{m_2 j}^{00}\right] A_{m_1 m_2} = 0$$

$$C_{m_1 m_2 ij} = C_{m_1 m_2 ij}^p + C_{m_1 m_2 ij}^I + C_{m_1 m_2 ij}^B$$

$$C_{m_1 m_2 ij}^p = \frac{E_{m_1 i}^{22} F_{m_2 j}^{00}}{s^4} + E_{m_1 i}^{00} F_{m_2 j}^{22} + \left(E_{m_1 i}^{20} F_{m_2 j}^{02} + E_{m_1 i}^{22} F_{m_2 j}^{20}\right) + \frac{2(1-v)}{s^2} E_{m_1 i}^{11} F_{m_2 j}^{11}$$

s is the aspect ratio of the plate $\frac{L}{L_1}$

$$C_{m_1 m_2 ij}^I = \sum_{p=1}^{4} \bar{k}_T \frac{\alpha_m(\xi_p)\alpha_i(\xi_p)F_{nj}^{00}}{s^4} + C_{m_1 m_2 ij}^{RJ}$$

$$C_{m_1 m_2 ij}^{RJ} = \bar{k}_\phi \left[\alpha'_{m_1}(0)\alpha'_i(0) - \alpha'_{m_1}(0)\alpha'_i(1) - \alpha'_{m_1}(1)\alpha'_i(0) + \alpha'_{m_1}(1)\alpha'_i(1)\right] F_{nj}^{00}$$

$$\lambda = \frac{\rho_s h \omega^2 L_1^4}{D} \qquad \bar{k}_\phi = \frac{k_\phi L_1}{D} \qquad \bar{k}_T = \frac{k_T L_1^3}{D}$$

$L = 2(L_2 + L_3)$ where L is the perimeter of the duct

$$E_{m_1 i}^{(r,s)} = \int_0^1 \alpha_{m_1}^{(r)}(\xi)\, \alpha_i^{(s)}(\xi)\ d\xi$$

$$F_{m_1 i}^{(r,s)} = \int_0^1 \beta_{m_1}^{(r)}(\eta)\, \beta_i^{(s)}(\eta)\ d\eta$$

Appendix B

$$I_{m_1 m_2 m_1' m_2'} = \int_0^L \int_0^{L_1} \int_0^L \int_0^{L_1} \sin\frac{m_1 \pi x}{L} \sin\frac{m_2 \pi x_1}{L_1}$$

$$\sin\frac{m_1' \pi x'}{L} \sin\frac{m_2' \pi x_1'}{L_1} \frac{\sin kR}{R} \, dx_1' \, dx' \, dx_1 \, dx$$

For self-radiation resistance $m_1 = m_1'$ and $m_2 = m_2'$

$$I_{m_1 m_2 m_1' m_2'} = \left\{ \frac{1}{\alpha_{m_1} \beta_{m_2}} J_1^{m_1 m_2} + J_2^{m_1 m_2} + \frac{1}{\alpha_{m_1}} J_3^{m_1 m_2} + \frac{1}{\beta_{m_2}} J_4^{m_1 m_2} \right\}$$

For mutual radiation resistance $m_1 \neq m_1'$ and $m_2 \neq m_2'$

$$I_{m_1 m_2 m_1' m_2'} = \frac{\varepsilon(m_1' - m_1)\varepsilon(m_2' - m_2)}{\left(\alpha_{m_1}^2 - \alpha_{m_1'}^2\right)\left(\beta_{m_2}^2 - \beta_{m_2'}^2\right)} \left\{ \alpha_{m_1} \beta_{m_2} J_1^{m_1' m_2'} - \alpha_{m_1} \beta_{m_2'} J_1^{m_1' m_2} \right.$$

$$\left. - \beta_{m_2} \alpha_{m_1'} J_1^{m_2' m_1} + \beta_{m_2'} \alpha_{m_1'} J_1^{m_1 m_2} \right\}$$

For $m_1 \neq m_1'$ and $m_2 = m_2'$

$$I_{m_1 m_2 m_1' m_2'} = \frac{\varepsilon(m_1' - m_1)}{\left(\alpha_{m_1}^2 - \alpha_{m_1'}^2\right)} \left\{ \alpha_{m_1} J_3^{m_1' m_2} - \alpha_{m_1'} J_3^{m_1 m_2} + \frac{\alpha_{m_1}}{\beta_{m_2}} J_1^{m_2' m_1} \right.$$

$$\left. - \frac{\alpha_{m_1'}}{\beta_{m_2}} \quad J_1^{m_1 m_2} \right\}$$

For $m_1 = m_1'$ and $m_2 \neq m_2'$

$$I_{m_1 m_2 m_1' m_2'} = \frac{\varepsilon(m_2' - m_2)}{\left(\beta_{m_2}^2 - \beta_{m_2'}^2\right)} \left\{ \beta_{m_2} J_4^{m_2' m_1} - \beta_{m_1'} J_4^{m_1 m_2} + \frac{\beta_{m_2}}{\alpha_{m_1}} J_1^{m_2' m_1} - \frac{\beta_{m_1'}}{\alpha_{m_2}} \quad J_1^{m_1 m_2} \right\}$$

$$\begin{Bmatrix} J_1^{m_1 m_2} \\ J_2^{m_1 m_2} \\ J_3^{m_1 m_2} \\ J_4^{m_1 m_2} \end{Bmatrix}$$

$$= \int_0^{L_2} \int_0^{L_1} \begin{Bmatrix} (L_1 - x)(L_2 - y) \\ (L_2 - y) \\ (L_1 - x) \end{Bmatrix} \times \begin{Bmatrix} \sin \alpha_{m_1} x \sin \beta_{m_2} y \\ \cos \alpha_{m_1} x \cos \beta_{m_2} y \\ \sin \alpha_{m_1} x \cos \beta_{m_2} y \\ \cos \alpha_{m_1} x \sin \beta_{m_2} y \end{Bmatrix} \frac{\sin k\sqrt{x^2 + y^2}}{\sqrt{x^2 + y^2}} dx \, dy$$

$\varepsilon(m_1' - m_1) = 1 \quad$ For $\quad m_1' = m_1$

$\qquad\qquad = 0 \quad$ for $\quad m_1' - m_1 = \pm 1, \pm 3, \pm 5, \ldots\ldots\ldots$

$\qquad\qquad = 2 \quad$ for $\quad m_1' - m_1 == \pm 2, \pm 4, \pm 6, \ldots\ldots$

$\alpha_{m_1} = \dfrac{m_1 \pi}{L_1}, \quad \beta_{m_2} = \dfrac{m_2 \pi}{L_2}$

Double integrals are expressed in single integrals by polar coordinate transformation.

$$\begin{Bmatrix} x \\ y \end{Bmatrix} = L_1 \rho \begin{Bmatrix} \cos(\theta) \\ \sin(\theta) \end{Bmatrix}$$

Double integrals can be rewritten as

$$\mathfrak{I}_{1i}^{m_1 m_2} = \int_0^{L_2} \int_0^{L_1} \sin \alpha_{m_1} x \sin \beta_{m_2} y \frac{\sin k\sqrt{x^2+y^2}}{\sqrt{x^2+y^2}} dx \, dy = \mathfrak{I}_{1i}^{(1)}\left(\alpha_{m_1}, \beta_{m_2}, L_1, L_2\right) +$$

$$\mathfrak{I}_{1i}^{(2)}\left(\alpha_{m_1}, \beta_{m_2}, L_1, L_2\right)$$

$$\mathfrak{I}_{2i}^{m_1 m_2} = \int_0^{L_2} \int_0^{L_1} \sin \alpha_{m_1} x \sin \beta_{m_2} y \frac{\sin k\sqrt{x^2+y^2}}{\sqrt{x^2+y^2}} dx \, dy = \mathfrak{I}_{2i}^{(1)}\left(\alpha_{m_1}, \beta_{m_2}, L_1, L_2\right) +$$

$$\mathfrak{I}_{2i}^{(2)}\left(\alpha_{m_1}, \beta_{m_2}, L_1, L_2\right)$$

$$\mathfrak{I}_{3i}^{m_1 m_2} = \int_0^{L_2} \int_0^{L_1} \sin \alpha_{m_1} x \sin \beta_{m_2} y \frac{\sin k\sqrt{x^2+y^2}}{\sqrt{x^2+y^2}} dx \, dy = \mathfrak{I}_{3i}^{(1)}\left(\alpha_{m_1}, \beta_{m_2}, L_1, L_2\right) +$$

$$\mathfrak{I}_{3i}^{(2)}\left(\alpha_{m_1},\beta_{m_2},L_1,L_2\right)$$

$$\mathfrak{I}_{4i}^{m_1 m_2} = \int_0^{L_2}\int_0^{L_1} \sin\alpha_{m_1}x \sin\beta_{m_2}y \frac{\sin k\sqrt{x^2+y^2}}{\sqrt{x^2+y^2}}\,dx\,dy = \mathfrak{I}_{4i}^{(1)}\left(\alpha_{m_1},\beta_{m_2},L_1,L_2\right) +$$

$$\mathfrak{I}_{4i}^{(2)}\left(\alpha_{m_1},\beta_{m_2},L_1,L_2\right)$$

Where

$$\mathfrak{I}_{1i}^{(1)} = \int_0^{\tan^{-1}\mu}\int_0^{\sec(\theta)} \sin\left(L_1\alpha_{m_1}\rho\cos\theta\right)\sin\left(L_1\beta_{m_2}\rho\cos\theta\right)L_1\,d\rho\,\,d\theta$$

$$\mathfrak{I}_{1i}^{(2)} = \int_{\tan^{-1}\mu}^{\frac{\pi}{2}}\int_0^{\csc\theta} \sin\left(L_1\alpha_{m_1}\rho\cos\theta\right)\sin\left(L_1\beta_{m_2}\rho\cos\theta\right)L_1\,d\rho\,\,d\theta$$

$$\mu = \frac{L_2}{L_1}.$$

$\mathfrak{I}_{2i}^{(1)}$, $\mathfrak{I}_{2i}^{(2)}$, $\mathfrak{I}_{3i}^{(1)}$, $\mathfrak{I}_{3i}^{(2)}$, $\mathfrak{I}_{4i}^{(1)}$, $\mathfrak{I}_{4i}^{(2)}$ are expressions similar to the above equations as $\mathfrak{I}_{1i}^{(1)}$ and $\mathfrak{I}_{1i}^{(2)}$

Further simplification of the above equations gives

$$\mathfrak{I}_{1i}^{(1)}$$

$$=\frac{1}{4}\int_0^{\tan^{-1}\mu}\left\{R\left(\alpha_{m_1},-\beta_{m_2},-k,\theta\right)+R\left(\alpha_{m_1},-\beta_{m_2},k,\theta\right)-R\left(\alpha_{m_1},\beta_{m_2},-k,\theta\right)\right.$$

$$\left.-R\left(\alpha_{m_1},\beta_{m_2},k,\theta\right)\right\}d\theta$$

$$\mathfrak{I}_{2i}^{(1)}$$

$$=\frac{1}{4}\int_0^{\tan^{-1}\mu}\left\{R\left(\alpha_{m_1},-\beta_{m_2},-k,\theta\right)+R\left(\alpha_{m_1},-\beta_{m_2},k,\theta\right)+R\left(\alpha_{m_1},\beta_{m_2},-k,\theta\right)\right.$$

$$\left.+R\left(\alpha_{m_1},\beta_{m_2},k,\theta\right)\right\}d\theta$$

$$\mathfrak{I}_{3i}^{(1)}$$

$$=\frac{1}{4}\int_0^{\tan^{-1}\mu}\left\{-S\left(\alpha_{m_1},-\beta_{m_2},-k,\theta\right)-S\left(\alpha_{m_1},-\beta_{m_2},k,\theta\right)-S\left(\alpha_{m_1},\beta_{m_2},-k,\theta\right)\right.$$

$$\left.-S\left(\alpha_{m_1},\beta_{m_2},k,\theta\right)\right\}d\theta$$

$$\mathfrak{I}_{4i}^{(1)}$$

$$= \frac{1}{4} \int_0^{\tan^{-1}\mu} \{S(\alpha_{m_1}, -\beta_{m_2}, -k, \theta) + S(\alpha_{m_1}, -\beta_{m_2}, k, \theta) - S(\alpha_{m_1}, \beta_{m_2}, -k, \theta)$$

$$- S(\alpha_{m_1}, \beta_{m_2}, k, \theta)\} \, d\theta$$

$$S(\alpha_{m_1}, \beta_{m_2}, k, \theta)$$

$$= \frac{\cos(L_1(\alpha_m \cos\theta + \beta \sin\theta + k)\sec\theta)}{(\alpha_m \cos\theta + \beta \sin\theta + k)} - \frac{1}{\alpha_m \cos\theta + \beta \sin\theta + k}$$

$$R(\alpha_{m_1}, \beta_{m_2}, k, \theta) = \frac{\sin(L_1(\alpha_m \cos\theta + \beta \sin\theta + k)\sec\theta)}{(\alpha_m \cos\theta + \beta \sin\theta + k)}$$

$$\mathfrak{I}_{ji}^{(2)}(\alpha_{m_1}, \beta_{m_2}, L_1, L_2) = \mathfrak{I}_{ji}^{(1)}(\alpha_{m_1}, \beta_{m_2}, L_1, L_2) \qquad j = (1,2)$$

$$\mathfrak{I}_{3i}^{(2)}(\alpha_{m_1}, \beta_{m_2}, L_1, L_2) = \mathfrak{I}_{4i}^{(1)}(\alpha_{m_1}, \beta_{m_2}, L_1, L_2)$$

$$\mathfrak{I}_{4i}^{(2)}(\alpha_{m_1}, \beta_{m_2}, L_1, L_2) = \mathfrak{I}_{3i}^{(1)}(\alpha_{m_1}, \beta_{m_2}, L_1, L_2)$$

$$J_{1i}^{m_1 m_2} = \mathfrak{I}_{1i}^{mn}, \quad J_{2i}^{m_1 m_2} = L_1 L_2 \mathfrak{I}_{2i}^{mn} - L_1 \frac{\partial}{\partial \beta_{m_2}} \mathfrak{I}_{4i}^{mn} - L_2 \frac{\partial}{\partial \beta_{m_2}} \mathfrak{I}_{3i}^{mn} +$$

$$\frac{\partial^2}{\partial \beta_{m_2} \partial \alpha_{m_1}} \mathfrak{I}_{1i}^{mn}$$

$$J_{3i}^{m_1 m_2} = L_2 \mathfrak{I}_{3i}^{mn} - \frac{\partial}{\partial \beta_{m_2}} \mathfrak{I}_{1i}^{mn}$$

$$J_{4i}^{m_1 m_2} = L_1 \mathfrak{I}_{4i}^{mn} - L_2 \frac{\partial}{\partial \alpha_{m_2}} \mathfrak{I}_{1i}^{mn}$$

These single integrals are evaluated numerically

References

[1] Istvan L.Ver, Leo L. Beranek, "Noise and Vibration Control Engineering Principles and Applications" *John Wiley & Sons,* (2006), Second edition, page 685

[2] A Johnson controls Company, "Fundamentals of Acoustics", *application guide.*

[3] A. Cummings, "Sound transmission through duct walls", *Journal of Sound and Vibration,* (2001), 239, 731-765

[4] Atkins Research and development Corp "The Control of noise in ventilation systems: A Designer's guide", *Taylor & Francis,* (1977), page 57

[5] A. Cummings, "Low frequency acoustic transmission through the walls of rectangular ducts", *Journal of Sound and Vibration*, (1978), 61, 327-345

[6] A. Cummings, I.-J. Chang, "Noise breakout from flat-oval ducts", *Journal of Sound and Vibration,* (1986), 106,17-33

[7] A. Cummings, I.-J. Chang , R.J. Astley, "Sound transmission at low frequencies through the walls of distorted circular ducts", *Journal of Sound and Vibration,* (1984), 97,261-286

[8] Wen L. Li and Howard J. Gibeling," Acoustic radiation from a rectangular plate reinforced by springs at arbitrary locations", *Journal of Sound and Vibration,* (1999), 220,117-133

[9] S. M. Kim and M. J. Brennan," A compact matrix formulation using the impedance and mobility approach for the analysis of structural -acoustic systems", *Journal of Sound and Vibration,* (1999), 223, 97-113

[10] B. Venkatesham, Mayank Tiwari & M. L. Munjal, "Prediction of breakout noise from a rectangular duct with compliant walls", *International Journal of Acoustics and Vibration,* (2011), 16, 180-190

[11] B. Venkatesham, Mayank Tiwari & M. L. Munjal, "Analysis & prediction of break-out noise from reactive rectangular plenum and four flexible walls", *Journal of Acoustical Society of America,* (2010), 128, 1789-1799

[12] C. E. Wallace, "Radiation resistance of a Rectangular Panel", *Journal of the Acoustical Society of America,* (1972), 51, 946–952

[13] Tian Ran Lin, Jie Pan "Vibration Characteristics of a Box-Type Structure" *Journal of Vibration and Acoustics, Transactions of ASME,* (2009), 131, 031004-1–031004-9

[14] Tian Ran Lin, Jie Pan, "Sound radiation characteristics of a box-type structure", *Journal of Sound and Vibration,* (2009), 325, 835–851

[15] W.H.Louisell,"Coupled mode and parametric electronics", *Wiley, New York,* (1960)

[16] W.L.Li ,"An Analytical solution for the Self-Mutual Radiation resistances of a rectangular plate", *Journal of sound and Vibration* (2001) 245(1),1-16

[17] R. J. Astley & Cummings ," A Finite Element Scheme for Acoustic Transmission through The Walls Of Rectangular Ducts Comparison With Experiment", *Journal of Sound and Vibration*(1984) 92(3), 387-409

[18] H.P Lee, "Natural frequencies and Mode shapes of Cylindrical Polygonal ducts", *Journal of sound and Vibration* (1993), 164, 182-187

[19] Pruthviraj Namdeo Chavan and B. Venkatesham," Free Vibration Analysis of HVAC Ducts", *Master's thesis,*2012

[20] ANSYS 13 *User guide,*ANSYS,Inc

[21] LMS Virtual Lab Rev 11, *User's Manual*

[22] RT Pro software   version 7 for PHOTON+,*User manual*, B&K

[23] m+p international SO Analyser Rev.4.1,*User manual*

[24] Hand –Held Analyzers Types 2250 and 2270 - *Technical Documentation*

[25] Sound Intensity Software BZ-7233 - *Technical documentation*

[26] Frank Fahy and John Walker ,"Fundamentals of Noise and Vibration", *E &FN Spon,*1998

[27] A.J. van Engelen ,"Sound radiation of a baffled plate:theoretical and numerical approach", *Research report,* January 2009